Master of Science Thesis

The effect of thermal fatigue on mechanical properties of thermoset composites

I.J. Bruinenberg

Faculty of Aerospace Engineering · Delft University of Technology

TU Delft Delft University of Technology

The effect of thermal fatigue on mechanical properties of thermoset composites

Master of Science Thesis

For obtaining the degree of Master of Science in Aerospace Engineering
at Delft University of Technology

I.J. Bruinenberg

20 June 2022

Faculty of Aerospace Engineering · Delft University of Technology

Delft University of Technology
Faculty of Aerospace Engineering
Department of Aerospace Structures and Materials

GRADUATION COMMITTEE

Dated: 20 June 2022

Chair holder:

Dr. D. Zarouchas

Committee members:

Dr.ir. O.K. Bergsma

Dr.ir. J.M.J.F. van Campen

Ir. R.J.C. Creemers

Abstract

Composite structures are used more frequently in newly designed aircrafts. This results in new difficulties compared to conventional metals during operational life. Especially, the material properties of two different materials can cause side effects, which are unwanted in a structure, for example thermal stresses. Many reports have been written about the difference in damage inflicted by thermal fatigue stresses compared to mechanical fatigue stresses. However, the environmental conditions and stacking sequences used in these reports are extreme and not common in aviation. This thesis focuses on the effect of combined thermal and mechanical fatigue load on the structural integrity of a laminate, but with realistic operations mechanical and environmental loads.

In-service F-16 data has been used to get a proper indication of the order of magnitude of mechanical and thermal forces applied on an aircraft during operations. These conditions are applied to a semi-quasi isotropic coupons, which were dominant in the 0 direction, to simulate a more common laminate for an aerospace structure. The residual transverse shear strength, residual bending strength, and stiffness are measured after a mechanical and/or thermal fatigue load has been applied to test specimens.

Results show no clear reduction for any of the measured material properties. The main differences in results can be derived from size differences in test coupons. However, all results are within the scattering region of the reference values. Thus, it can be concluded that the structural integrity of a laminate will not be affected negatively by a combined thermal and mechanical fatigue load, if the conditions match the used operational circumstances.

Contents

List of Figures

List of Tables

Chapter 1

Introduction

Since 1903 technology developments in aviation have not stopped. The first aircraft was built in a static fail design (safe-life concept). There was no management on damage during service, it was a static strength design. The aircraft should withstand the maximum forces during flight. This concept was good enough, because of the low amount of flights. However, when the flights became longer and more regular fatigue became more important, in 1953 the first fatigue regulation article 4b. 270 was released [1]. This is the start of the fatigue regulations in aviation and the introduction of multiple load paths (fail-safe design), which ultimately has led to the damage tolerance (safety-by-inspection) principle in 1978. A structure can have damage, even from the first time loads are applied. However, a structural design with this principle expects damage (growth) and that it can be found (with a proper inspection schedule), before the damage can lead to failure of the structure [1]. Currently, aircrafts are designed with all the three different design principles for an optimized safety design:

- Safe-life
- Fail-safe
- Damage tolerant

Additionally, the development of material has not stopped since the start of aviation. The brothers Wright started with a wooden airplane. During WW1 metal aircrafts were invented and used, resulting in increased popularity of all-metal constructed airplanes from 1919 up to 1934. During the 1960s composites were used more extensively [2], eventually leading to the Boeing B-787 Dreamliner and Airbus A350 with the highest composite mass usage in civil aviation. Approximately 50% of the B-787 total mass consists of composite and about 80% when measured in volume, because of the reduction in weight [3].

Nowadays, materials have to be cost efficient in terms of production and durable to reduce the overall cost. Mechanical fatigue tests are commonly used to predict the life cycle of conventional aerospace metals. Due to the homogeneous nature of metals it is adequate to perform only mechanical fatigue tests, but for composite materials thermal fatigue may actu-

ally become an issue as well. Composites are manufactured are manufactured from different materials (resin and fibers) with different material properties, and each material reacts differently to mechanical stresses, but also to temperature changes. Especially, the effects of temperature changes on the life cycle of composite are important to research. During flight operations, aircrafts are subjected to large temperature changes. The temperature at cruising altitude (-50°C) is much lower than normal ground temperature (23°C). Within the certification process this environmental factor is taken into account with a "knock-down" factor. However, this is a factor based on static tests under adverse environmental conditions, but it does not consider repeated thermal cycling nor does it consider correlation effects between thermal cycling and mechanical load cycling.

To conclude, composite structure are used more in aviation in different temperature ranges, while only considering a static environment "knock-down" factor in the design phase. Thermal fatigue tests are not mandatory to perform, however the correlation of thermal and mechanical fatigue is still unknown. To understand the influence of thermal fatigue on a composite structure research needs to be performed on the life cycle of a composite laminate considering thermal fatigue.

Chapter 2

Literature review

2.1 Thermal Stresses in Composites

This paragraph contains information about thermal stresses in composite based on a literature study. A composite structure can be made with different manufacturing methods; for example Resin Transfer Molding, Vacuum Injection, or Vacuum Molding [4]. There are various sorts of fibers (carbon or glass fibers) and matrices (thermoplastic or thermoset) that can be used in a composite for a specific design. The direction of the fibers can also be used to strengthen the composite in a specific direction. All these variations are having an effect on the thermal stresses in a composite laminate, because each material has his own coefficient of thermal expansion (CTE) in each of the principle directions. This coefficient determines how much the material will increase or decrease in volume due to temperature changes.

2.1.1 Introduction of thermal stresses

Common composite are formed by heating up both matrix and fibers to higher temperatures. Thermosets are heated to a lower temperature compared to thermoplastics. Thermoplastics are heated up to the glass transition or melting temperature, while thermoplastic composites are solidified by cooling. Thermoplastics can be re-melted by increasing the temperature above its melting temperature. This is different compared to thermoset composites. Thermosets are solidified by a chemical reaction (i.e. cross-linking of molecules) during curing, which is a permanent irreversible process. Both types of composites have thermal residual stresses, caused by the manufacturing process. Additionally, thermal stresses may occur during service, because of the temperature differences that may occur during the life of an aircraft. These stresses exist on three different levels [5][6].

- On micro-mechanical level, the mismatch in coefficient of thermal expansion causes a mismatch in volumetric shrinkage between the fiber and matrix, resulting in thermal residual stresses.
- On macro-mechanical level, a ply has a coefficient of thermal expansion in the transverse

and longitudinal direction, which can be calculated by the rule of mixture. Therefore, the shrinkage is different in each direction during cooling. However, the shrinkage is mechanically constrained by other plies within the laminate. For example, the 90 degree ply in a cross-ply composite constrains the shrinkage of the 0 degree ply in transverse direction. These mechanical constraints on ply-to-ply level are causing residual stresses. If a laminate is not balanced, deformation (curvature) of the laminate can occur during curing. After the laminate is cured, the same effect is responsible for the development of additional thermal stresses, caused by temperature differences during the life of the aircraft.

- On laminate level, the cooling rate of a thermoplastic laminate is different on the surface compared to the center of the laminate. The surface solidifies faster than the center, resulting in a shrinkage constraint imposed on the center plies caused by the surface plies. The difference in cooling rate is not important for a thermoset composite. Thermoset composites solidify during a chemical reaction at a specific constant temperature level.

These thermal stresses can cause different defects in a composite laminate after manufacturing [7][8]:

- Fiber and tow misalignment can occur during the curing process. If the fibers experience an axial load, caused by thermal residual stresses, while the matrix is unable to provide support in the transverse direction, fiber deformation and waviness will occur.
- Transverse ply cracking (microcracks) can be initiated by thermal residual stresses. When the thermal residual stresses exceed the strength of the resin and/or fiber-matrix bonding strength, small matrix cracks or matrix-fiber debonding can occur. The kind of defect is depending on the matrix-fiber bond strength. A very strong bond will cause matrix cracking, while a more weak bond causes the crack to propagate along the fiber-matrix interface. The crack initiates at the vicinity of the free edge, where the thermal stress can be locally high. The microcracks are a important starting point for the further growth of fatigue cracks during fatigue life. Research has shown that mechanical fatigue life (S/N curve) is longer when a lower curing temperature is used. The lower temperature difference between the curing temperature and in-service temperature imposes a lower thermal residual stress. Therefore, a lower curing temperature causes less microcracking, resulting in a longer fatigue life [9].
- If the consolidation of a thermoplastic composite was not adequate, delamination at the free edge can occur. This edge delamination is associated with high interlaminar stress development by discontinuity of materials throughout the thickness of a laminate.
- Warpage is one of the additional defects that can occur due to thermal residual stresses. Especially, thin unsymmetrical laminate are sensitive to warpage. However, unsymmetrical laminates are not commonly used in structures.

2.1.2 Thermal Expansion Coefficient

There has been research [10] on the use of polyether etherketone (PEEK) as a matrix and the effect of different fiber stiffness on the CTE of unidirectional composite. A qualitative inspection for the amount of defects has been performed on each specimen. A Non-Destructive

Inspection method, i.e. C-scan, has been used to ensure that the test results are not affected. The expected volume changes are very low, because the CTE itself also has a low value. Therefore, a measurement instrument which can accurately measure small displacements is needed. In this experiment a Fizeau interferometer with a helium neon lazer is used, because of the accuracy up to 5 nanometers. The CTE value in the transverse direction is larger than in the axial direction, because its coefficient is matrix dominated. Less accurate equipment is therefore suitable in transverse direction. In this specific experiment a Perkin-Elmer TMA push-rod dilatometer is used, which can measure changes up to 0.4 micrometers.

Figure 2.1 shows that the CTE of PEEK is linear dependent on the temperature. It is important to notice that the Tg is not yet reached in this figure. After Tg, the curve of the CTE loses its linearity, because of the change in viscoelasticity of the material and the CTE will increase more. The CTE of the matrix changes depending on the temperature, while the CTE of the fiber is independent of the temperature. The two CTEs combined results in an overall CTE of the composite. This combined CTE is not a linear curve anymore, but more "bath tub" curve with scattering at higher temperatures (figure 2.2).

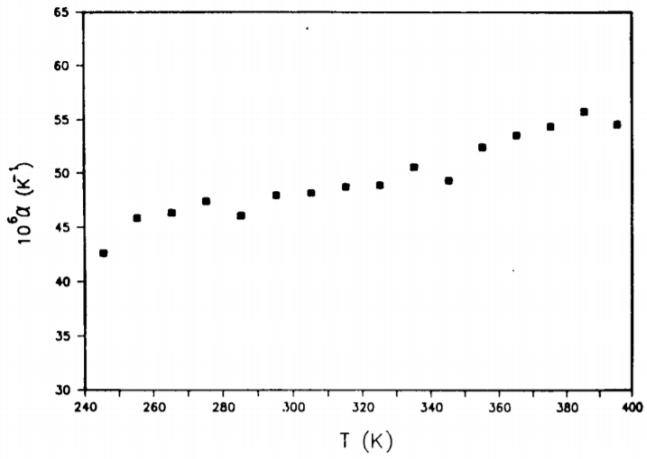

Figure 2.1: Thermal expansion coefficient of PEEK depending on the temperature. [10]

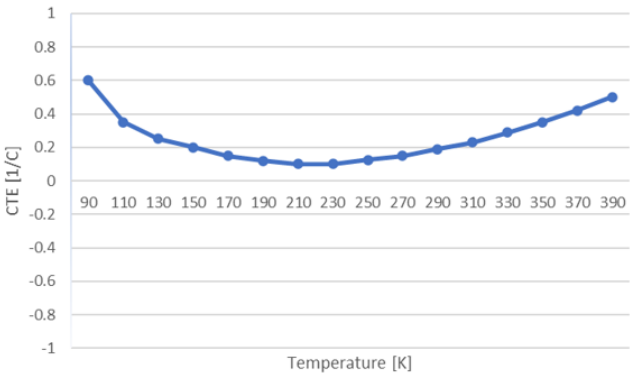

Figure 2.2: Thermal expansion coefficient of AS4/PEEK UD laminate parallel to the fiber direction. Recreated from "Thermal expansion behaviour of thermoplastic composite materials" by J A Barnes et al. [10].

This curve can be explained the Rule of Mixture and the viscoelasticity of the matrix. The Rule of Mixture can be used to calculate the CTEs of the ply, which can be seen in appendix A.1 and A.2. This results in the following two CTEs formula for the fiber direction (α_{11}) and the transverse direction (α_{22}).

$$\alpha_{11} = \alpha_{f11} * \frac{1}{\frac{1-V_f}{V_f} * \frac{E_m}{E_{f11}} + 1} + \alpha_m * \frac{1}{\frac{V_f}{1-V_f} * \frac{E_{f11}}{E_m} + 1} \tag{2.1}$$

$$\alpha_{22} = \alpha_m * (1 - V_f) + \alpha_{f22} * V_f \tag{2.2}$$

Both formula are depending on the volume fraction and the difference between the CTE of the fiber and matrix. The transverse CTE is more dominated by the CTE of the matrix, because the stiffness ratio is not a factor for the CTE of the ply. However, the stiffness ratio is an important factor in the CTE formula in the fiber direction. This ratio is a representation of the amount that the matrix is restricted in thermal expansion by the stiffer fiber.

The force P_m (2.3) in the calculation of the laminate CTE (appendix A.1) is the curing force caused by the change in temperature.

$$P_m = \frac{A_f * E_{f11}}{\frac{V_f}{V_m} * \frac{E_{f11}}{E_m} + 1} * \Delta T(\alpha_m - \alpha_{f11}) \tag{2.3}$$

This can be divided by the surface to get the curing stresses within the fibers (appendix A.1).

$$\sigma_f = \frac{E_f}{\frac{V_f}{1-V_f} * \frac{E_f}{E_m} + 1} * \Delta T(\alpha_m - \alpha_{f11}) \tag{2.4}$$

Curing takes place at elevated temperatures. When cooled down to room temperature the temperature difference becomes negative, resulting in compressive stresses on the fiber and tensile stresses on the matrix. Important to notice is that these curing stresses are not taking into account in the classical laminate theory. The formula above describes curing stresses in the fiber direction in a single ply (micro-level). The classical laminate theory starts with a homogeneous ply, which is initially free of stress. The homogeneous ply has different CTEs in each direction. When different plies are cured together, a curing stress is induced into the laminate (macro-level). The classical laminate theory considers these macro-level curing stresses, however not the initial thermal stresses on micro-level. The "offset" of micro-level stresses could be important to considered, if it leads to transverse crack initiation.

Figure 2.2 shows the a CTE curve of a unidirectional CFRP/PEEK ply parallel to the fiber direction. The stiffness of the matrix changes within the temperature range. At lower temperatures the stiffness of the matrix is higher, but the stiffness of the fiber does not change. Therefore, the stiffness ratio is also changing throughout the temperature range. The CTE of PEEK is also changing throughout the temperature ranges. With the assumption that at very low levels the matrix starts to become very stiff, it is possible to get the "bath tube" curve from the given equation. Important to notice is the scatter at temperatures in the higher range. The reason is unknown yet. The other tests in the paper did not have this scattering.

The influence of fiber stiffness on the CTE was researched with several fibers (table 2.1 and 2.2). A very stiff fiber results in a lower CTE of the composite (comparing figures 2.2 and 2.3),

which can be confirmed by the CTE formula in the fiber direction. A stiffer fiber decreases the stiffness ratio on the α_{f11} side, resulting in a more fiber CTE dominant outcome.

Table 2.1: CTEs of fibers at room temperature. [10]

Reinforcement	Linear CTE (x 10^6 m/m/K) at 23°C
Hercules AS4	0.24
Experimental	0.24
Hercules IM7	-0.16
Thornel P75	-0.97
Thornel P100	-0.96

Table 2.2: Material properties of fiber laminates. [10]

Reinforcement	Fiber Tensile Modulus GPa	Fiber Volume Fraction %
Hercules AS4	234	62
Experimental	234	62
Hercules IM7	303	62
Thornel P75	524	55
Thornel P100	724	45

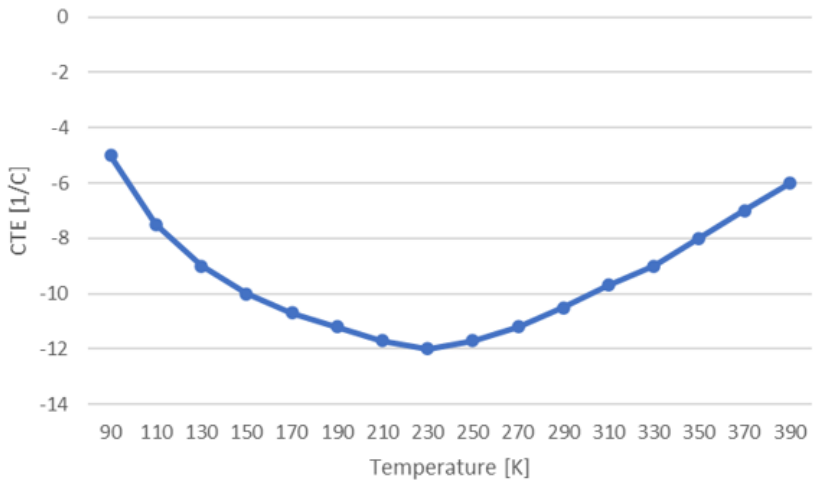

Figure 2.3: Thermal expansion coefficient of P75/PEEK UD laminate parallel to the fiber direction. Recreated from "Thermal expansion behaviour of thermoplastic composite materials" by J A Barnes et al. [10]

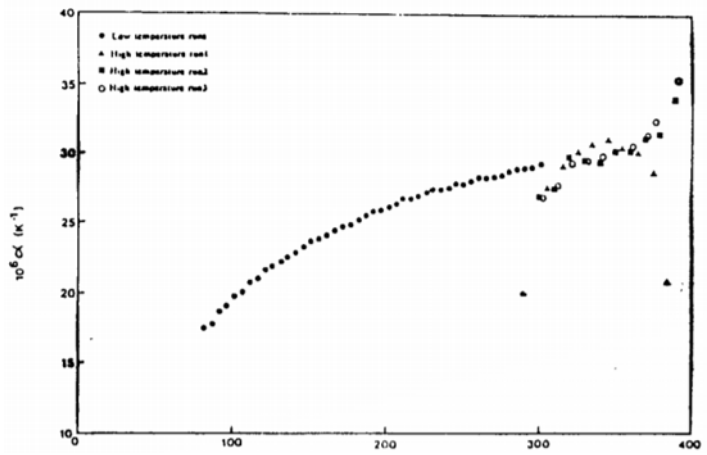

Figure 2.4: Thermal expansion coefficient of PEEK transverse to the fiber direction [10].

The curve transverse to the fiber directions is more dominated by the CTE of the matrix. The CTE curve plotted in figure 2.4 is looking much more like the CTE of PEEK alone compared to the "bath tube" curve. This can be explained by the formula of α_{22}. The stiffness ratio has no impact on the CTE of the ply, which results in a more matrix dominant CTE. The scattering in the higher temperature region is caused by free-volume annealing at higher temperatures for extended amount of time. This causes a change in material behaviour and influences the CTE.

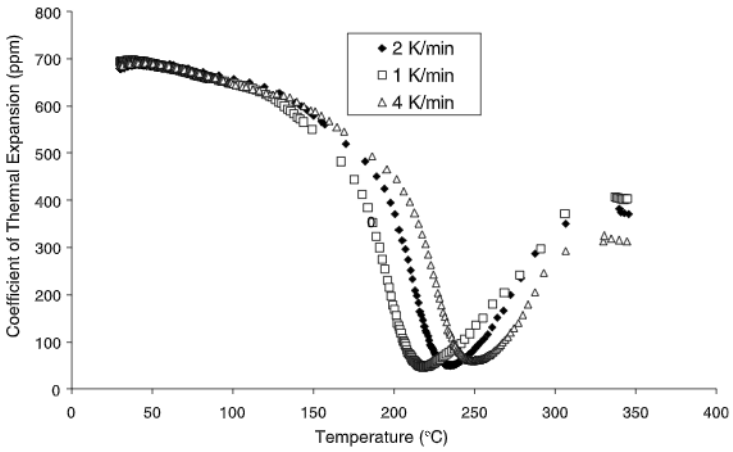

Figure 2.5: Thermal expansion coefficient of a thermosetting composite during curing depending on the temperature. [11]

For thermoplastic composite the thermal expansion coefficient changes throughout the operational temperature range. However, the thermal expansion coefficient also changes slightly during the curing process of a thermosetting (dicyanate ester) composite [11]. Figure 2.5 from E. Leroy's et al. research shows that a dip in the thermal expansion coefficient occurs at the gelification temperature. The location of the dip is depending on the heating rate during the curing process. This dip can be explained further with figure 2.6. At the start of the curing process the CTE drops strongly, caused by size growing of molecules due to volemetric shrinkage. Further on, at 50-60% of the curing process the gelification point has

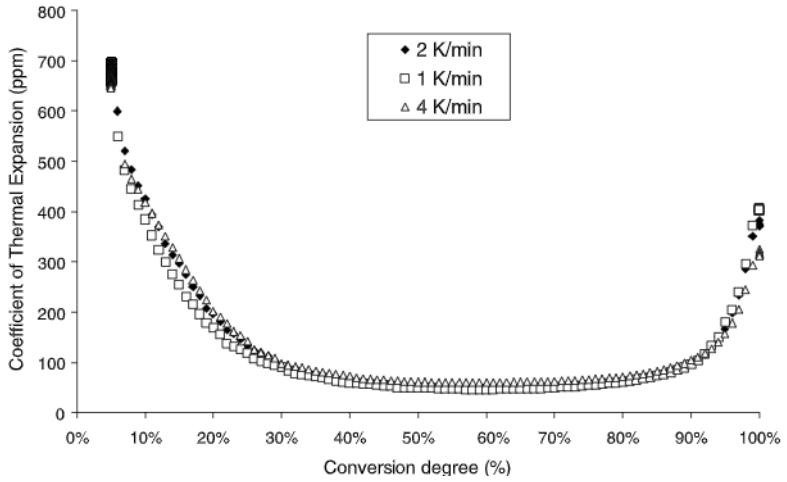

Figure 2.6: Thermal expansion coefficient of a thermosetting composite during curing depending on the conversion degree. [11]

been reached. Here, the change in CTE is lower then 100 ppm, which is in absolute value almost zero. At this point the resin starts to transform to a solid from a viscous material. At the more higher degree of conversion vitrification starts to occur and the specific volume of cyanate esters grows, resulting in an increase of CTE.

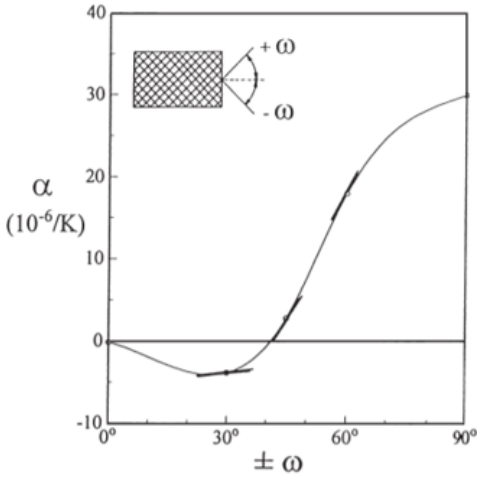

Figure 2.7: Thermal expansion coefficient depending on the fiber direction. [12]

Unidirectional laminates are not commonly used in structures. These kind of laminates are very strong in the fiber direction, but not in any other direction. However, off-axis and multi-axial loads can be in introduced into structures. A structure made of only unidirectional laminates cannot withstand these stresses. Therefore, structures with complex loads have different fiber directions to endure loads in different directions. The stacking sequence determines the CTE of laminate, because all the different plies have an influence on the CTE of the principle axes of the whole laminate [12][13]. Figure 2.7 shows the CTE curve of a carbon fiber reinforced polymer (CFRP) depending on the stacking direction. Remarkable to notice is the minimum at $\pm$ 30 degrees in the curve. This dip is caused by the difference in CTE between the fiber and transverse direction. The transverse expansion of the $+\alpha$ ply causes stresses in the $-\alpha$ ply. If these stresses are not parallel to the fibers in the $-\alpha$ ply, shear stresses will occur on ply level. All these shear forces together, result in shearing deformation. Shear deformation is elongation in one direction and shortening in the other one. The classical laminate theory confirms this phenomenon. A principle axial load causes tensile stresses in the fibers, but also in-plane shear stresses. These shear stresses cause shear deformations on ply level. And shear deformations on the ply level are on the laminate level characterized by elongation in one direction, but shortening in the other direction. This explains how an increase of the temperature can still result in shrinkage (and an apparent negative CTE) for certain laminate lay-ups; the thermal stresses in such laminates consist of stresses in fiber direction, but also of in-plane shear stresses on the different plies.

2.2 Parameters influencing the CTE

Besides temperature itself, the thermal expansion coefficent is also depending on other parameters [12]:

- Annealing
- Thermal cycling
- Creep

To measure these parameters, an interferometric laser dilatometer with a resolution of 316 nanometer is used in this experiment [12]. This setup has a lower resolution then the one used in the previous experiment [10] (5 nanometer), however the results do not need to be more accurate than 316 nanometer.

2.2.1 Annealing

Annealing of polymers has multiple different purposes like desorption of water, relaxation of curing stresses, and increasing the crystallinity volume of semi-crystaline polymers. However, research has shown that annealing also has very minimal effect on the CTE (2.8) at the lower temperature region. The difference in the higher temperature regions can be neglected.

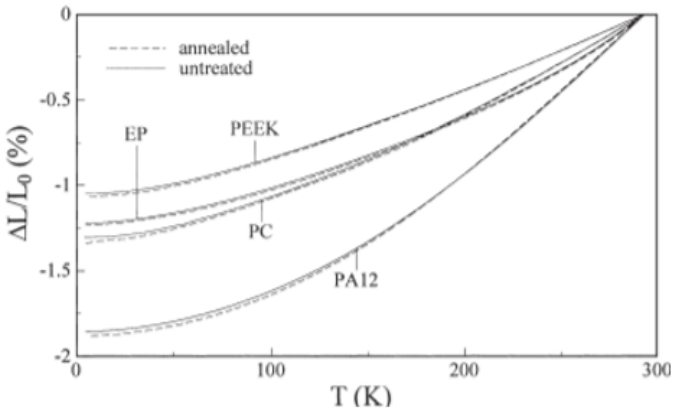

Figure 2.8: The influence of annealing on the CTE depending on the temperature. [12]

2.2.2 Thermal cycling

The test specimens (FT 700/EP) with a ± 30 degree lay-up are thermally cycled from -196°C up to 20°C (room temperature) 100 times. The shear forces at this stacking sequence cause a high negative thermal expansion, resulting in a large effect induced by the thermal cycling. This phenomenon is already discussed in paragraph 2.1 and shown in figure 2.7. Figure 2.9 shows the influence of thermal cycling on the specimens on the expansion compared to the original length. The percentile change can go up to 20% at lower temperatures. Intralaminar and interlaminar cracks are forming due to the shear and thermal stresses at the interface between two materials and plies. These cracks reduce the ability of transferring the shear forces to another ply, which led to a strain closer to zero. The crack propagation will be discussed in paragraph 2.5.

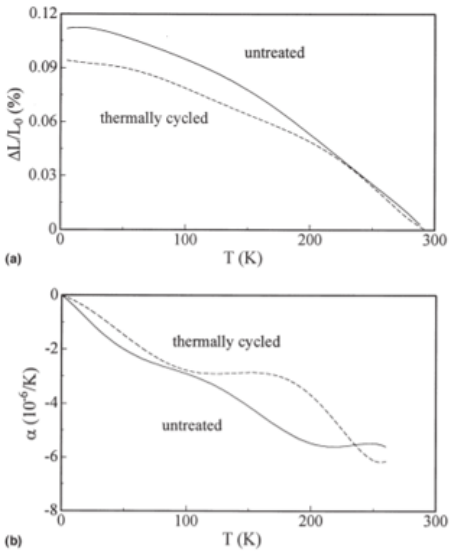

Figure 2.9: The influence of thermal cycling on (a) strain and (b) on the thermal expansion coefficient depending on the temperature. [12]

2.2.3 Creep

Changes in thermal expansion coefficient can be explained with the Classical Laminate Theory and figure 2.10. Figure 2.7 has shown that a change in the fiber direction can cause a difference in CTE in accordance with with the Classical Laminate Theory. The figure displays the test results of laminates (T 800/EP) with different ply directions (±30, ±45, and ±60) that had a constant compression force of 150Mpa for 20 hours long in the 0 degree direction prior to the thermal test. All the test samples are showing a change in strain. The change due to creep for the ±30 and ±60 laminates is in terms of percentages small. The ±45 laminate was influenced a lot by the creep force in terms of percentages. However, the absolute value of the changes are small for all stacking sequences. The increasing strain difference between the ±30 and ±60 laminate can be explained by the large change in CTE, caused by the more dominant influence of matrix properties in the rule of mixture. The right side of the graphs is confirming the transformation from a negative CTE (±30 degree) to a positive CTE (above ±45 degrees) shown in figure 2.10.

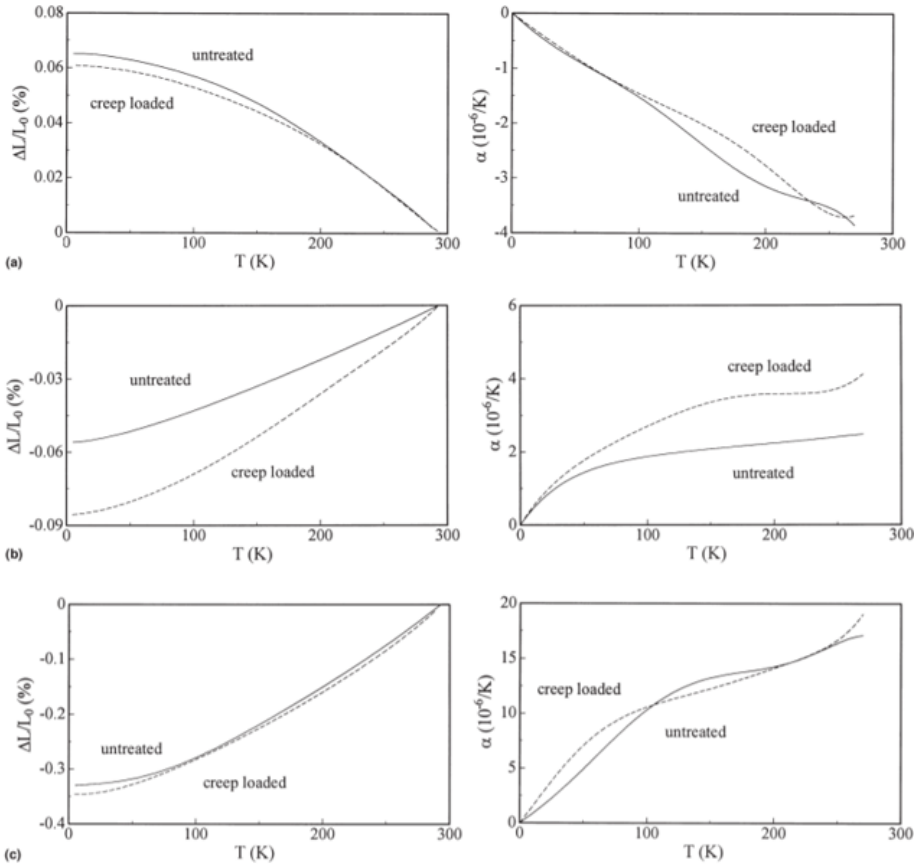

Figure 2.10: The influence of creep on the thermal expansion coefficient before and after a compressive creep loading.(left side: strain, right side: coefficient of thermal expansion). (a) $\omega \pm 30$; (b) $\omega \pm 45$; (c) $\omega \pm 60$ [12].

It is important to notice that these results are depending on the material. These test are representative for structures with these specific fibers and matrix. However, if another matrix or fiber is used, the material properties will also be different. So the influence of creep on CTE will change.

2.3 Thermal fatigue

In the previous paragraph the influence of thermal cycling on the thermal expansion coefficient was mentioned. The cracks formed due to the different stress levels caused by temperature differences, resulting in the decrease of stress transfer between the matrix and fiber, because of the poor interface between the two materials or between different ply directions (delamination). This is an example of thermal fatigue.

The definition of thermal fatigue is: 'Thermal fatigue is the gradual deterioration and eventual cracking of a material by alternate heating and cooling during which free thermal expansion is partially or completely constrained.'[14]. The opposite of thermal fatigue is isothermal fatigue. This is a low-cycle fatigue where the temperature is constant through the cycle. Thermal fatigue is a broad definition, which can be divided further into thermal mechanical fatigue and thermal stress fatigue. These two types of fatigue are distinguished by external and internal constrains. If a material is under thermal mechanical fatigue, it has stresses caused by temperature changes while being forced in the same volume. The material wants to deform, but it is not allowed by the boundary conditions. On the other hand, thermal stress fatigue are stresses within the material caused by two materials with different CTEs interfering due to temperature changes.

Thermal stress fatigue analysis is very important for composite materials and structures. The advantage of using different materials and using the best material properties of each of them, causes a disadvantage in thermal aspects. A large difference in CTE induces a large stress. These stresses are always present in composite materials, because of the curing process. Formula 2.5 shows the mathematical reasons [15] on laminate matrix level for multi-axial laminates, caused by the expansion due to temperature changes. This formula does not apply to unidirectional laminates. Additionally, this formula assumes that the stiffness of the fiber is much higher than the matrix. The curing stresses on ply level were already shown in formula 2.4

$$\sigma_{matrix} = \Delta\alpha * \Delta T * E_{matrix} \tag{2.5}$$

Where:
σ = Thermal stress in [MPa]
$\Delta\alpha$ = Difference in CTE between two materials [m/m/K]
ΔT = Temperature difference $(T_0 - T_1)$ [K]
E_{matrix} = Modulus of the matrix [GPA]

In paragraph 2.1.1 transverse cracking caused by thermal residual stresses after curing was already mentioned. Aircraft experience also thermal cycling in normal operational conditions [16],[17]. These temperature changes during in-service operation also impose stresses due to a mismatch in CTE. J. Ju and Roger J. Morgan proves this in "Characterization of Microcrack Development in BMI-Carbon Fiber Composite under Stress and Thermal Cycling"[18]. A

BMI-Carbon laminate (5250-4/IM7) was thermally cycled within three regions: -196-23°C, 23-250°C, -196-250°C. During the thermal cycle two different bending load levels were applied resulting in a bending stress of 718 MPa (0,406% strain) and 1.49 GPa (0,843% strain). These loads are used to compare the crack density of a thermally cycled specimen with the reference graph from a specimen where only a bending load was applied.

The largest temperature cycle (-196-250°C) causes the most significant microcrack development (figure 2.12), due to the large difference in temperature. The extreme change in temperature causes fiber-matrix interface failure at higher temperatures and matrix cracking at lower temperatures. The crack density is much higher in two thermally cycled laminates (23-250°C and -196-250°C) compared to the reference density. The value of the bending load becomes more important, when a large temperature cycle is used. Additionally, the crack density increases if the temperature cycle approaches the glass transition temperature (T_g) (figure 2.13), caused by a decrease of fiber-matrix strength.

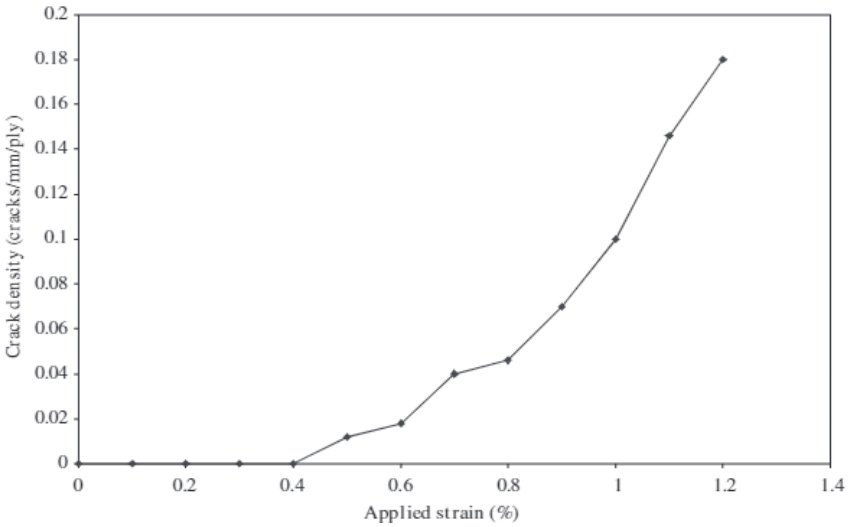

Figure 2.11: Transverse crack density of a 5250-4/IM7 composite as a function of the applied bending strain, used as a reference graph. [18].

2.4 Thermal fatigue compared to mechanical fatigue

The previous paragraph has described the influence thermal fatigue can have on a structure with a constant mechanical load. During in-service operation mechanical fatigue has also an important role for the structural integrity. Therefore, mechanical fatigue has an important role in the certification and the use of an aircraft. However, the importancy of thermal fatigue should not be neglected. C. Henaff-Gardin and M.C. Lafarie-Frenot compared mechanical and thermal fatigue on cross-ply T300/914 laminates $(0_n/90_n)_s$ and $(90_n/0_n)_s$ [19]. The specimens are cycled between -50 and 150 degrees with 4 degrees each minute in the thermal tests. The mechanical fatigue test consists of a mechanical cycling load with a maximum amplitude equal to 50% of the static failure load (365 MPa) in the fiber direction. The test was designed such that a comparable stress amplitude would be applied for $sigma_{22}$ in the 90 ply during the two fatigue tests (thermal and mechanical). After completion of the fatigue test the crack density in the 90 ply was measured.

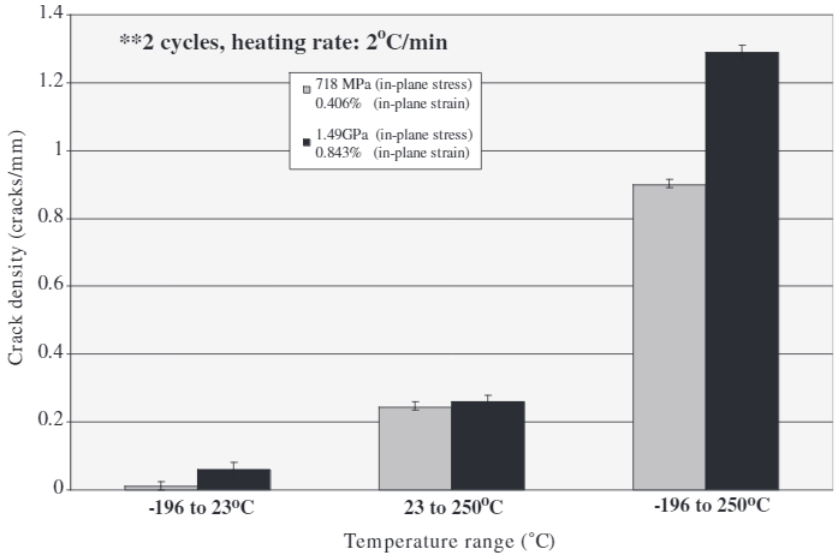

Figure 2.12: Microcrack density of a 5250-4/IM7 composite for three different temperature regions and two bending strains [18].

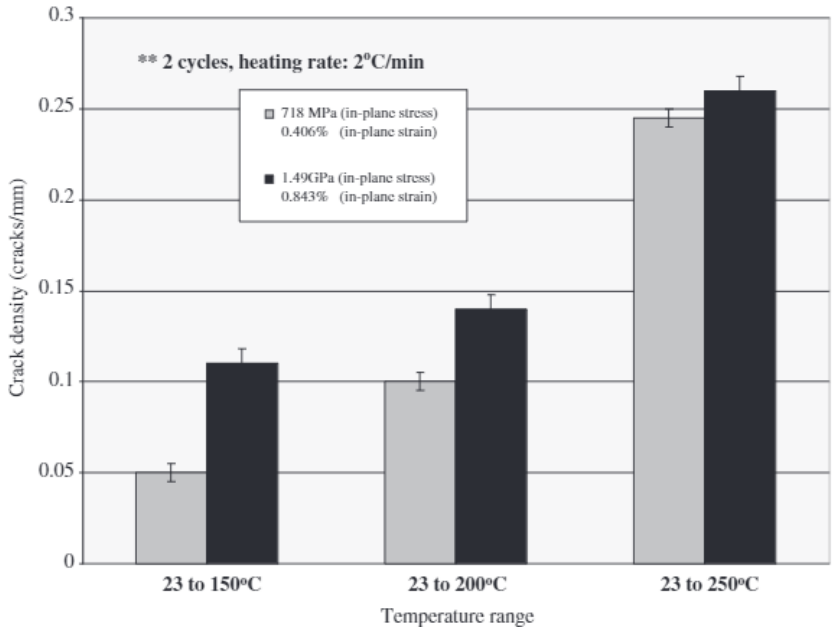

Figure 2.13: Microcrack density of a 5250-4/IM7 composite for three different temperature regions and two bending strains [18].

The stresses in each direction were estimated using thermoelastic analysis (table 2.3). However, edge effects, viscoelasticity of materials at higher temperatures and changes in thermal properties are not included in this estimation. Therefore, it is a rough estimation.

The absolute stresses in the σ_{11} and σ_{22} direction are the same in thermal fatigue due to the biaxial stresses. The minimum stress value is higher in mechanical fatigue, because of the the thermal residual stresses. The stresses σ_{22} for the 0 ply are also lower compared to the 90 ply

Table 2.3: Stresses in 0 and 90 layers for $(0_n/90_n)_s$ and $(90_n/0_n)_s$ laminates in thermal and mechanical fatigue tests [19].

		$\sigma_{22}90°(MPa)$	$\sigma_{11}90°(MPa)$	$\sigma_{22}0°(MPa)$	$\sigma_{11}0°(MPa)$
Mechanical fatigue	Thermal residual stress (20°C)	36,7	-36,7	36,7	-36,7
	Minimum mechanical stress	4.3	-1.3	1.3	685,9
	cyclic stress amplitude	38,5	-11,5	11,5	617,3
Thermal fatigue	Minimum thermal stress (-50°C)	6,9	-6,9	6,9	-6,9
	Cyclic stress amplitude	45,9	-45,9	45,9	-45,9

during mechanical fatigue. Important to notice is the high tensile stress that is ply.

Table 2.4: Ultimate crack density at the edge of the 90 layer in $(90_3/0_3)_s$ and $(0_3/90_3)_s$ laminates under thermal en mechanical fatigue loads [19].

	$(0_3/90_3)_s$ internal layer	$(90_3/0_3)_s$ external layer
Mechanical fatigue ($2{\cdot}10^6$ cycles)	0,94±0,05 (cracks/mm)	0,43±0,02 (cracks/mm)
Thermal fatigue (500 cycles)	0,84±0,05 (cracks/mm)	0,46±0,02 (cracks/mm)

Table 2.4 shows the crack density at the edge of the 90 layer in the two different stacking sequences per fatigue test. The crack densities in each layer are in the same order of magnitude for the mechanical and thermal fatigue tests, but when the 90 ply is positioned as the internal layer a higher crack density is found than when the 90 ply is positioned as the external layer. The internal layer has a higher crack density after both fatigue tests. However, the most striking result is that fatigue, causes the same damage within a test sample as mechanical fatigue within so many fewer cycles (500 compared to $2{\cdot}10^6$ cycles). It seems that cracks develop much easier due to thermal fatigue compared to mechanical fatigue.

Figure 2.14 shows the cracked surface area per unit volume in every layer during the mechanical and thermal fatigue test. Important to notice is that the cracked surface in the internal and external layers are the same for $(90_3/0_3)_s$ and $(0_3/90_3)_s$ during thermal fatigue, because of the same biaxial stresses in each of the stacking sequence. This graph cleary shows that the saturation points are on the same level. However, the amount of cycles needed to reach this saturation point is very different. There are only 500 thermal cycles needed in comparison to the 10.000 mechanical cycles. Thermal fatigue is in the beginning of the life cycle more intensive and thus creating more cracks in the laminate at an early stage. During an accumulative damage analysis both types of fatigue should be considered. If the life cycle analysis only uses the mechanical fatigue component, the chance is that the laminate

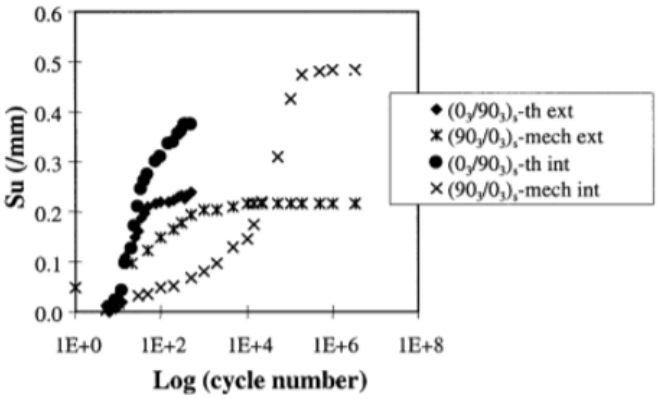

Figure 2.14: Crack density measured per cycle at internal and external plies for thermal and mechanical fatigue test [19].

will fail sooner than expected due to the thermal fatigue component. However, it is unknown yet what the curve and expected life cycle will be when both types of fatigues are interfering with each other. Is it possible just to add both types of damage into one curve? Or should we consider a certain factor which increases or decreases the overall damage? Important to notice is the difference in damage between the external and internal ply. This phenomenon will be discussed in a later part of this report.

2.4.1 Frequency

The comparison between mechanical and thermal fatigue should consider the difference in frequency used in a test. The cracks that are forming during both tests are intralaminar transverse matrix cracks (along the fibre) that progress as interlaminar cracks or delaminations. The material properties of the matrix determines in what stage of the life cycle the cracks occur. The most important property is viscoelasticity. The value of viscoelasticity determines how much a material acts like a solid material or like a fluid depending on the stress applied. In this experiment the matrix is not a solid or a fluid, but somewhere in between (more to the solid properties). The frequency used has an important factor in the end results due to the viscoelasticity of the material. A higher frequency will make the material act more elastic. The material does not have the "time" to fully adapt to the forces. So with a lower cycle speed the material has more "time" to fully absorp the whole force. The influence of the frequency on the damage during life cycle can be seen in figure 2.15. The amount of cracks per length increases when the frequency of the mechanical fatigue cycle is decreased. However, even when the frequency is the same as the thermal fatigue cycle, the damage done by the mechanical fatigue is still significantly lower. The frequency of the fatigue cycle is important, but also the kind of fatigue should be considered.

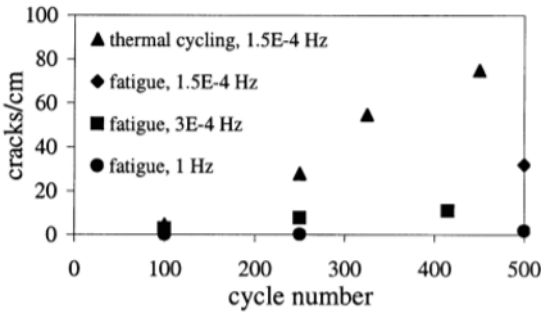

Figure 2.15: The effect of frequency on the cracking density during mechanical fatigue [19].

2.4.2 Influence of stacking sequence on thermal fatigue

In the previous paragraph the influence of the stacking sequence on the crack density is shortly mentioned. M.C. Lafarie-Frenot has researched the impact of the free edge on thermal cycling [20]. The experiment uses multiple cross-ply coupons, which were cut out of one big $(0/90)_s$ laminate, to ensure the specimens had the same manufacture process. The coupons were cut in three different ways (figure 2.16). This approach makes sure that it is possible to research different stacking sequences, while being cut form the same laminate.

All coupons are cycled from -50 degrees up to 150 degrees 1000 times. At various moments the crack density is measured using X-ray. The direction of the fibers compared to the free edge and the location within the stacking sequence is important to interlaminar cracks. The cracks can be seen in figure 2.17. Remarkable is that there are no cracks when the internal ply is cut in a 45 degree angle. However, the 90 angle cut ply does crack when it is a internal ply. The combination can be seen in the octagonal coupon in the bottom right of figure 2.17.

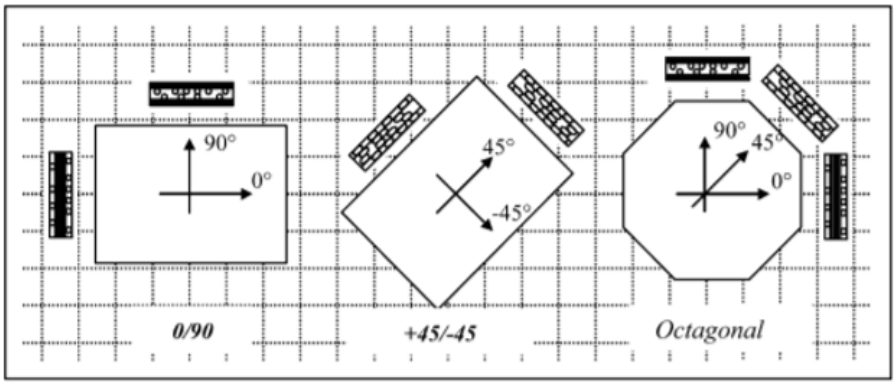

Figure 2.16: Stacking sequence and geometry of the test coupons [20].

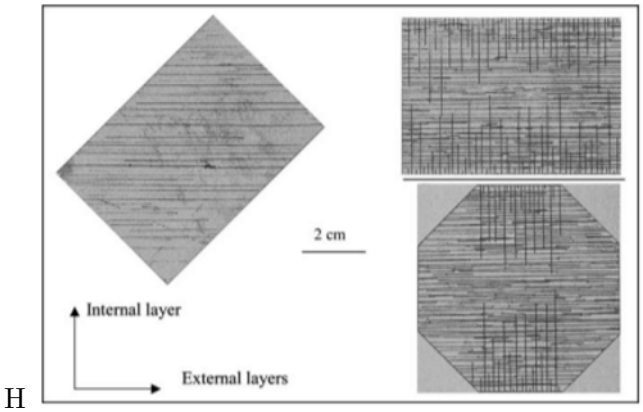

H

Figure 2.17: X-rays of coupons after 1000 thermal cycles.

The laminate does not crack in the areas where the fibers are cut at 45 degrees. But the cracks do appear when the fibers are perpendicular to the edge. The crack density in the external plies is very constant, when looked at the octagonal specimen. The angle between the free edge and the fibers has less of an influence and the cracks are crossing the whole laminate. Both aspects are different for the internal ply. Figure 2.18 shows the results of the crack density counting. In the graph there is a clear difference between the internal and the external plies depending on the fiber direction at that specific location.

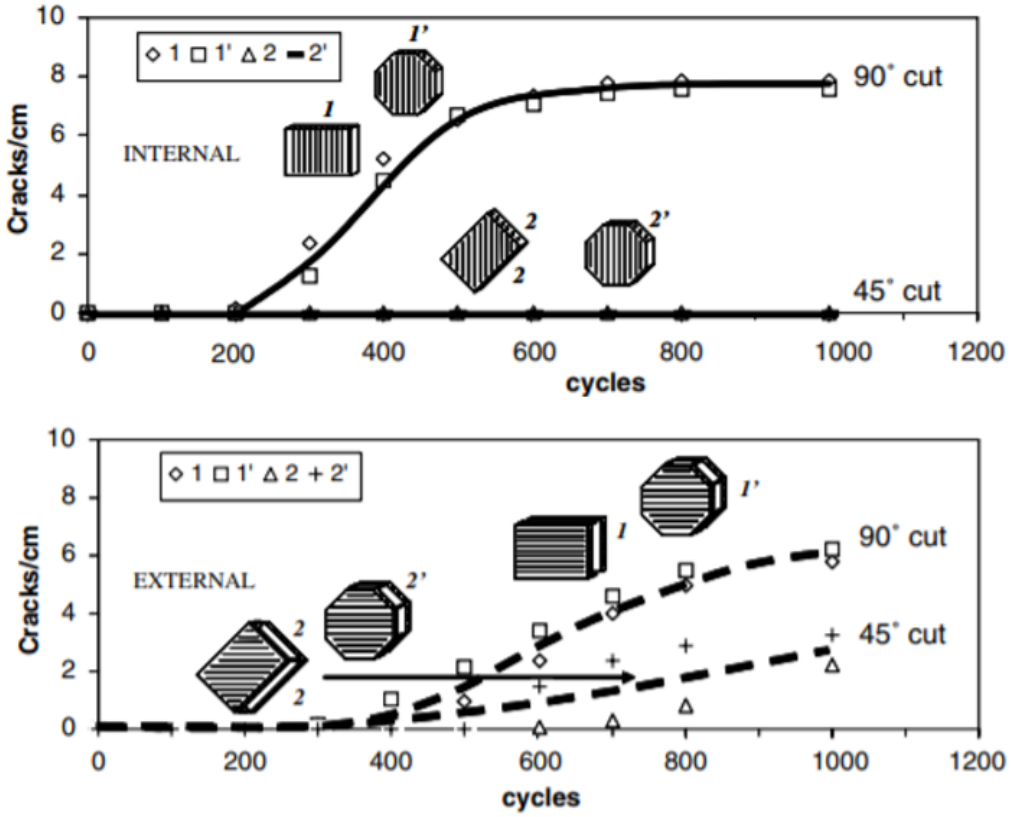

Figure 2.18: The crack density internal and external plies with different fiber direction depending on the amount of thermal cycles [20].

The reason that the internal plies do not crack when they are cut under +45 or -45 degrees, can be explained by the edge stresses. Figure 2.19 shows the transverse thermal stresses at the edge of an octagonal laminate, calculated by a FEM simulation, depending on the distance from the edge. The values at 0 mm edge distance are varying a lot. Especially, the ±45 cut plies have a low transverse stress. However, when the edge is perpendicular to the fiber there is a high thermal transverse stress, which can cause crack initiation and thus the crack density will be higher in those plies. Apparently, the low transverse stress in the ±45 degree cut plies is not enough to create a crack initiation for the internal plies. The stresses increases further from the edge, however cracks are more likely to start at the edge, resulting in the crack distribution showed in figures 2.17 and 2.18. For the external ply a possible explanation is the combination of interlaminar shear stresses and peel stresses at the edge of the specimen, resulting in bending stresses in the external ply. This could lead to crack initiation.

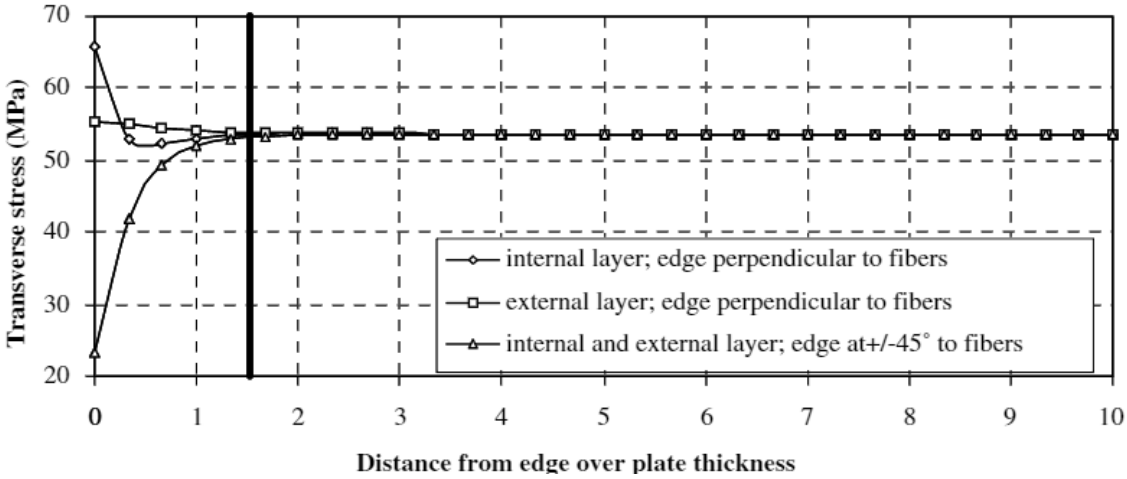

Figure 2.19: FEM simulation of thermal transverse ply stresses in a octagonal laminate at -50°C [20].

Thus, the stacking sequence is important in the thermal fatigue life cycle. The coupons that were used are simple stacking sequence (cross ply). To know if the stacking sequence is as important as stated, a test with more diverse stacking sequence should be performed. It is unknown how much of an influence the stacking sequence on the crack density and fatigue life has in other sequences. Is the curve going gradually from the 45 degree internal ply to the 90 degree curves? Or are there certain directions which are better than others?

2.5 Damage propagation

In the previous paragraph the crack density was discussed. However, this value does not fully determine the residual strength. The type of crack is also important for the mechanical properties. S, Kobayashi, K. Terada, S. Ogihara, and N. Takeda did a damage analysis of matrix cracking in CFRP composites [21]. $[0_2/90_4/0_2]$ coupons are thermically cycled from -196 degrees up to 250 degrees. These are very extreme temperatures and are not normal for composite in aerospace operation. These temperatures are more likely in space operations. However, this experiment clearly shows how a crack evolves within a laminate.

The cracks in the 0 ply start at the free edge and propagate through the thickness of the ply up to a ply with another direction (figure 2.20). Stacking multiple plies with the same direction has no positive impact in stopping the crack. The same phenomenon can be seen in the four 90 plies. The cracks in the internal ply (90 direction) start at the tip of the 0 ply crack and at the free edge. There is a large stress concentration at the crossing point of both cracks (0 and 90 direction). At this point delamination between the 0 en 90 ply starts to occur. This phenomon was also described by C. Henaff-Gardin and M.C. Lafarie-Frenot [19]. J.Ju and Roger J. Morgan show that even the heating/cooling rate has an impact on the change of failure mode [18]. The failure mode during thermal cycling with an applied bending load went from a transverse cracking to inter-ply delamination, when the cooling/heating rate was changed from 2°C/min to 7°C/min. Especially, delamination decreases the mechanical properties of the laminate. If the residual strength is lower than the applied force, it will fail.

Bending strength is probably a good measurement for the amount of delamination damage.

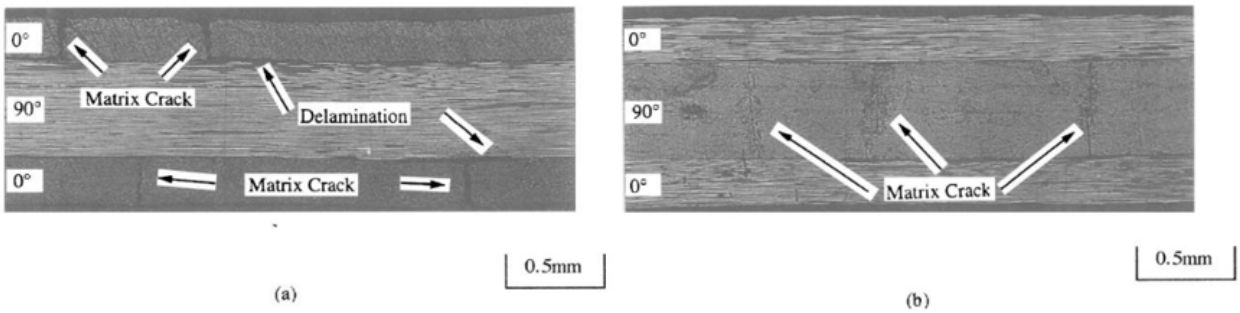

Figure 2.20: Side-view X-rays of the laminate showing cracks through the thickness.(a) parallel to the 0 direction; (b) parallel to the 90 direction [19].

Figure 2.21 confirms that laminates have a saturation point of cracks due to thermal fatigue. If the laminate has cracked enough, both material (fiber and matrix) can expand and shrink without creating stress in the material beside it. But the saturation point proves that a laminate will not fail from only thermal fatigue, it has to have an additional force applied to fully fail the whole laminate. The importancy of the stacking sequence is confirmed in figure 2.21 as well. The crack density in the internal ply is about two times higher than in the external ply. The factor two can be confirmed by the difference in edges stresses in a internal and external ply (figure 2.19). But the crack density curve also is depended on the amplitude of the thermal cycle. A higher amplitude value will create a steeper crack density curve.

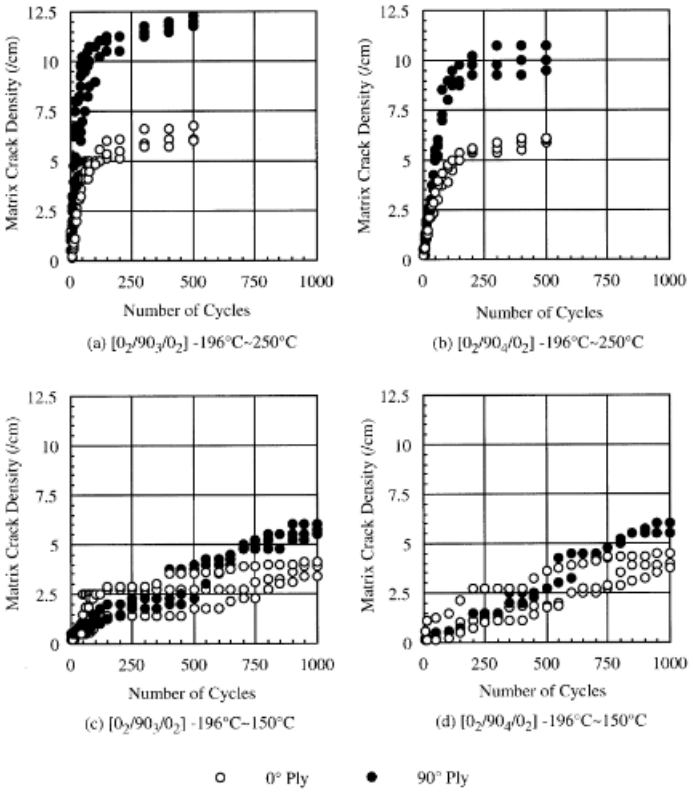

Figure 2.21: Crack density saturation point in the external and internal ply depending on the amplitude of the temperature cycle [19].

Chapter 3

Research question, objective and aims

The material properties of a composite can cause problems during in-service operations. The mismatch of the coefficient of thermal expansion between fibers and matrix may introduce multiple different defects like delamination, fiber and tow misalignment, and transverse ply cracking. All these defects are due to thermal stresses on micro-mechanical, macro-mechanical or laminate level, depending on the differences in material properties between the materials. Therefore, these defects start immediately after manufacturing, caused by the so-called "curing stresses". Possible defects during service due to temperature changes is just an outcome of the same princip problem.

Several articles have described that the CTE of a composite may change depending on the temperature. The rule of mixture explains the dependency. The CTE is dominated by volume-fraction combined with the stiffness. This stiffness changes within the operation temperature range due to viscoelasticity of the matrix. Additionally, the CTE changes even during the curing process. However, the variation in CTE during curing should not be considered. For operational service it does not matter what happens during curing, the end state after the curing process is the important starting point for operational service. As previously stated aircrafts are operating at different temperature as a consequence of the variation in altitude. However, the extreme lower temperature of -196 °C that has been used in many of the papers on thermal stresses is not common in normal airline and military operations. These exterme temperatures should not be tested. On the other hand, the change in CTE in a normal operation temperature range should be considered, because this has a direct influence on thermal stresses and possibly on crack development and residual strength.

As previously stated, thermal stresses can cause delamination and transverse ply cracking. Multiple articles have described the amount of crack density within a ply with no mechanical force, a constant bending force, and cycling mechanical force combined or compared with a thermal fatigue load. The crack density is an important aspect in the residual strength of a laminate. Intra-laminar transverse cracks and interlaminar delaminations are expected to have a large influence on the residual bending strength and shear strength of a laminate. Therefore it is expected that bending strength and shear strength are a good measure for the

amount of damage in such a specimen. The test results can vary with the kind of defects within a laminate. Delamination decreases the residual bending and interlaminar shear strength. In principle, transverse ply cracking is less problematic in a bending or interlaminar shear test, but the cracks may start as an initiator for delamination cracking after all. However, the (ultimate) strength is not the only important aspect. A specimen with a high crack density can still function under normal in-plane loading. The deformation of a composite has an important role for the structural integrity. Parts are designed to a specific geometry and are most of the time not allowed to change a lot. The stiffness of a part should be considered as well, and a certain amount of stiffness reduction is a clear sign of damage in the specimen. So, also stiffness could be used as measure for the amount of damage in the specimens.

Another aspect is the stacking sequences used in the various experiments. Most of the laminates were cross-ply laminate, while these kind of stacking sequences are not commonly used in aircrafts structures due to the lack of strength in the off-axis. The thermal stresses imposed by ply-on-ply constraints (marco-mechanical level) are different in a cross-ply compared to a more complex laminates. Cross-ply laminate have higher stresses in the transverse direction in the matrix than laminates with smaller fiber angles, because a peak of transverse stresses occurs at angle difference of 90°. It is to be expected that more complex laminates will have the same overall amount of transverse ply cracks (formula 2.5), but the angle of the edge cut should be considered. Composite structure are not likely to be rectangle, but have different edge angles in one structure. Figures 2.18 and 2.17 confirm that the results of crack density are completely different when 45° cuts are added. It is still unsure what happens when for example 30° and 60° cuts are mixed with 0°, 90° and 45° cut angles. However, it is not necessary to research this, because 30° and 60° plies are not common in structures.

The comparison between mechanical and thermal fatigue should be researched more. Crack density increases in a lower amount of cycles during thermal fatigue than due to mechanical fatigue. The slope of the crack density curve versus the amount of cycles is an important indicator on how fast the strength threshold can be reached. A laminate can reach its crack saturation point in a very low amount of cycles due to thermal fatigue. On the other hand, the amount of load cycles of mechanical and thermal loads is different. For example, during an operational flight of an airliner, just one thermal cycling load will be applied. But the structure will endure many mechanical cycles. For military aircraft this thermal cycling spectrum will be different. Military aircrafts are more likely to change altitude during operation. However, the expected life cycle of an airline is longer and thus thermal fatigue can still be an important factor to consider.

The combined effect of mechanical and thermal fatigue has not been researched properly. As previously stated, some reports compare the difference between the two sorts of fatigue separately, but also when thermal fatigue is combined with a constant mechanical load or mechanical fatigue. The saturation point of the crack density is important. This level will be determined by the loading amplitude of the cycle. But it is still uncertain what will happen to the saturation point if the two fatigue cycles alternate each other. Is the saturation point determined by the highest amplitude cycle or is it a combination of both cycles and how fast is that point reached?

To conclude, thermal stresses are important in the life cycle of certain laminates, but there are more aspects to consider. A structure with high stress levels and a high amount of damage within, could still perform its function. Therefore, the focus should be on the structural

integrity of a structure.

The structural integrity is the ability that a structure does not fail or deform in such a way that the structure can no longer fulfill its function. So the deformation during load is also a important aspect to consider. For example a blade may not brake, but if it deforms in such a way that it does not guide the air enough, it still loses it function. The following question needs to be answered to have a better understanding of thermal fatigue in aerospace structures:

- How will the structural integrity of a structure develop with a combined and realistic thermal and mechanical load spectrum, applied during the life cycle of a representative laminate used in aerospace structures?

With sub-questions:

- In which stage of the life cycle does thermal and mechanical fatigue have the most impact on the residual bending strength and interlaminar shear strength?
- How is the stiffness of a laminate affected due to mechanical and thermal fatigue?
- Does the combination of mechanical and thermal fatigue have a negative impact on the residual strength during the life cycle of a laminate?

Chapter 4

Theoretical content and methodology

4.1 Background

There has been a lot of research on crack density caused by mechanical or thermal fatigue. However, as previously stated, there are still unknown aspects. Further experiments are needed to fill these "gaps". The experiments should answer, if the structural integrity and residual strength changes due to a combination of thermal and mechanical fatigue. Especially, the combination of the two fatigue loads is important to research.

As stated in the introduction of this report, currently most structures in aerospace are designed with the damage tolerance principle. A proper inspection schedule is, therefore, important. Matrix cracks in composites generally do not lead to ultimate failure under in-plane loading conditions, because the fibers are still intact and are able to carry the (in-plane) loads, and final failure is a fiber dominated phenomenon. Under out-of-plane loading conditions, however, matrix cracks do have a significant effect on the residual strength. The residual strength of composite structures with barely visible impact damage (BVID) is a critical design criterion. If the residual strength is below operation load and it is not possible to detect a defect, an unwanted failure can occur. Impact strength is a matrix dominated property. Therefore, transverse matrix cracking could have a negative influence on the residual strength and is not easily detectable. If a composite has a high density transverse matrix cracks, it could influence the impact damage evolution negatively and thus result in a lower residual impact strength, imposing a higher safety risk on the aircraft.

4.2 Methodology

The residual strength and stiffness are aspects of the integrity of a structure. In the case that thermal and mechanical fatigue damage will not change the residual strength, it still could change the stiffness, which can have a negative influence on the fatigue life or even the functionality of a structure. Bending strength tests and shear strength tests are prime candidates to detect such loss of strength or stiffness caused by matrix cracks, because they

are respectively fiber and matrix dominated tests. Besides these two tests, an impact damage test is also a candidate considering the matrix dominated failure. However, impact damage test has more scattering. To properly see the difference a test with less scatter is preferred. It is expected that the specimen will have intralaminar cracks and by which the residual bending and interlaminar shear strength would decrease. While, performing the test the amount of deformation needs to be measured. The elastic reaction can be different, while the flexural strength is the same in each of the fatigue cycles.

4.3 F-16 data analysis

Military aircrafts have a broader operational scope compared to a normal airline usage spectrum. In military operations aircrafts change altitude more often and have a dynamic flight plan. Therefore, it is more interesting to have an insight in the order of magnitude of induced stresses of fighter aircrafts. The data used consists of real F-16 strain gauges data from the root of the wing. The raw data set is based on 34 different F-16 flights and averaged in different ways for mechanical and thermal load. This can be done due to the fundamental set up of the experiment with a constant load amplitude. The assumption has been made that the loads in a composite structure are the same as in the metallic structure of the F-16, which can be done because the usage pattern of newly designed military fighter aircrafts are comparable to F-16s. Secondly, the thickness of the composite structure is assumed to be approximately equal to metallic structure. However, this is only to get an order of magnitude of the stress levels in a structure as a starting point.

The data is divided into 2 parts. 1) The tensile stress data, derived from strain data from strain gauges at the root of the wing. 2) General flight data such as speed, altitude, and air temperature. The data was already filtered by a Peak-Valley-Peak filter. From the filtered data it is possible to make three different mechanical and thermal loading spectrums depending on the severity of usage, which can be seen in the graphs below.

- Average load cycle – This is a cycle which takes the average stress level of all peaks and valleys during flight (between take-off and landing) of all 34 flights.
- Average Max/Min cycle – This is the average of the maximum and minimum stress level during flight of all 34 flights.
- Extreme Max/Min cycle – This is the maximum and minimum of stress level recorded during flight of all flights.

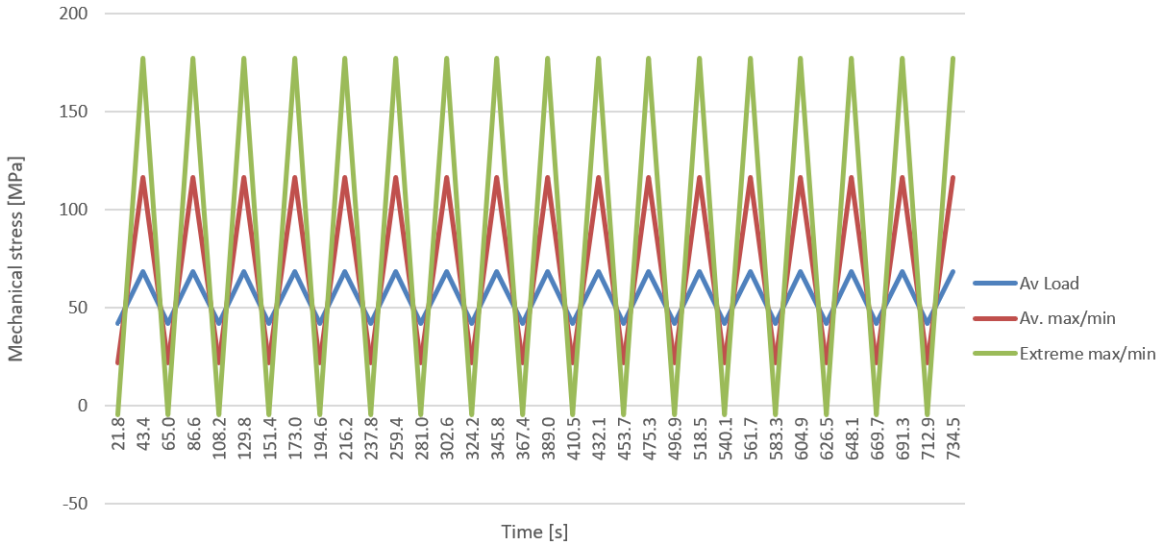

Figure 4.1: Mechanical fatigue options based on real F-16 data.

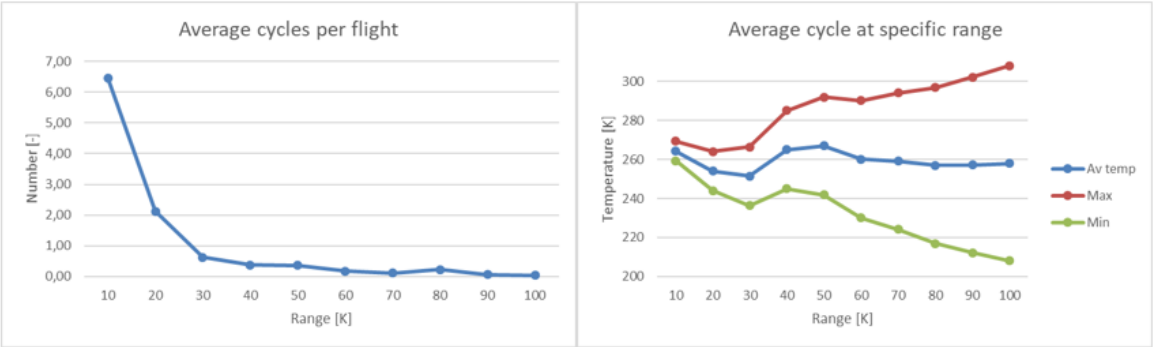

Figure 4.2: Thermal cycling loads based on real F-16 data.

The average time between two peaks is around 43 seconds in figure 4.1. Taking this 43 seconds with a general life time of 1.000.000 cycles gives a fatigue life of 12.000 FH. A normal fatigue life of a military fighter is around 10.000 FH (which is equal to 850.000 fatigue cycles). A slow fatigue frequency is more severe than a fast fatigue frequency, because the material has more time to fully develop the stresses within the material. This in combination with the viscoelastic behaviour of the matrix causes delayed cracking in a laminate [19].

For the thermal load rainflow counting method is used to count the amount of times the temperature changed a lot (above 5 [K]) as the data was not filtered. The amplitude changes are grouped from 10 to 100 in steps of 10 [K]. The mean value is estimated by taking the average of all mean values in a specific range group.

4.3.1 Mechanical load

In the previous paragraph the different load cycles were already mentioned as a starting point. For each loading case a difference in stresses with and without curing stresses are made. Curing stresses occur based on the temperature difference between T_g and usages

temperature, which is room temperature for the mechanical load. However, there will also be relaxation of stresses if the laminates are rested for a while. The amount of relaxation is uncertain. Therefore, it is hard to calculate the curing stresses exactly. In reality the curing stresses are somewhere in between the 23.9 and 0 MPa, but most likely closer to the 23.9 MPa than 0 MPa.

The S_{22T} according to the material properties of a UD ply is 48,9 MPa. The S_{22T} of a semi-quasi isotropic laminate $(45/-45/0/90/0/45/-45/90/0/90/45/-45/0)_s$ can be calculated with the classical laminate theory. The maximum stress of scenario 3 (with 177 MPa) is already higher than 48,9 MPa. Additionally, the amount of strain 0,33% is also large. Scenario 3 would be a to severe loading cycle. Scenario 2 has a strain of 0,22% and a maximum stress level of 40,5 MPa. The 0,22% strain is a good strain level to choose as it will most likely cause fatigue damage. Normal limit load strains are between 0,2% and 0,24%. This means that scenario 2 (117 MPa) can be used as a proper mechanical fatigue load for a composite structure.

Table 4.1: σ_{22} depending on the mechanical fatigue load and curing stresses.

	117 [MPa] with curing	117 [MPa] without curing	177 [MPa] with curing	177 [MPa] without curing
Curing stresses (RT)	23,9 [MPa]	0 [MPa]	23,9 [MPa]	0 [MPa]
Mechanical minimum stresses	0 [MPa]	0 [MPa]	0 [MPa]	0 [MPa]
Mechanical maximum stresses	16,6 [MPa]	16,6 [MPa]	25,1 [MPa]	25,1 [MPa]
Mechanical minimum strain	0 [-]	0 [-]	0 [-]	0 [-]
Mechanical maximum strain	0,0022 [-]	0,0022 [-]	0,0033 [-]	0,0033 [-]
Overall minimum stresses	23,9 [MPa]	0 [MPa]	23,9 [MPa]	0 [MPa]
Overall maximum stresses	40,5 [MPa]	16,6 [MPa]	49,0 [MPa]	25,1 [MPa]
Mean stress value	32,2 [Mpa]	8,3 [MPa]	36,45 [MPa]	25,1 [MPa]
Amplitude	8,3 [MPa]	8,3 [MPa]	12,55 [MPa]	12,55 [MPa]

4.3.2 Thermal load

Beside a mechanical load there will be also a thermal fatigue load applied to the specimen to simulate in-service operations. As expected there are more small temperature changes during flight compared to large ones. The large changes are a result from take-off and landing. The small temperature differences are happening mid-flight. The small (up to 10 [K]) temperature differences, cause a small change in stress level. Material also needs time to adapt to the new temperature. To simplify the experiment for time efficient reasons only the take-off and landing cycle will be a thermal loading cycle. This can be done, because it is the most severe thermal load applied on the structure.

In table 4.2 two different scenarios are stated with each a differences in stress levels with and without curing stresses. Again relaxation has an influence on the stress levels and thus is it not possible to calculate the precise stress values.

The thermal loading cycle from 306K to 223K (range of 83K) is comparable to the thermal data from the F-16. Figure 4.2 displays that take-off and landing range is different for each flight. The average amount of cycles per flight with a temperature range difference from 50K up to 100K is 0.94. This means that almost every flight a temperature range difference between 50K and 100K occurs during take-off and landing. Scenario 1 uses a temperature range of 80K, which is in the middle of a very conservative and severe approximation.

Table 4.2 displays that the stress values of 306K to 223K are almost the same as the stress

values of scenario 2 of the mechanical load. This would be highly preferable to compare the different fatigue load with each other. However, the demand of the climate chamber and operation cost are high. Because of time and cost efficient planning it was not possible to run the climate chamber on this specific temperature range. The temperature range used is from 353K to 213K, which is a larger range. Fortunately, the difference in maximum stress level for the plies within the laminate is small. The difference in minimum stress level is bigger, because the lower end of the thermal stresses (high temperature) will approach the T_g temperature, resulting in a lower mean stress value and a higher amplitude. This could cause a faster increase in damage during fatigue life, however this thermal fatigue load can still be used in the experiment as lower cycle counters are considered in the experiment.

Table 4.2: σ_{22} depending on the thermal fatigue load and curing stresses with room temperature as reference temperature.

	306K to 223K with curing	306K to 223K without curing	353K to 213K with curing	353K to 213K without curing
Curing stresses (RT)	23,9 [MPa]	0 [MPa]	23,9 [MPa]	0 [MPa]
Thermal minimum stresses	-2,2 [MPa]	-2,2 [MPa]	-12,5 [MPa]	-12,5 [MPa]
Thermal maximum stresses	16,1 [MPa]	16,1 [MPa]	18,3 [MPa]	18,3 [MPa]
Thermal minimum strain	0,00002 [-]	0,00002 [-]	0,00012 [-]	0,00012 [-]
Thermal maximum strain	-0,00015 [-]	-0,00015 [-]	-0,00017 [-]	-0,00017 [-]
Overall minimum stresses	21,7 [MPa]	-2.2 [MPa]	11.4 [MPa]	-12.5 [MPa]
Overall maximum stresses	40 [MPa]	16,1 [MPa]	42,2 [MPa]	18.3 [MPa]
Mean stress value	30.85 [Mpa]	6.95 [MPa]	26,8 [Mpa]	2,9 [MPa]
Amplitude	9.15 [MPa]	9.15 [MPa]	15,4 [MPa]	15,4 [MPa]

4.4 Experimental set-up

4.4.1 Experimental test plan

The experiment consist of multiple parts. Firstly, a strength and stiffness baseline has to be made. Secondly, the specimens are subjected to tensile fatigue and/or thermal fatigue. Lastly, all specimen are tested in residual strength and stiffness. With these experiments it is possible to see the impact of thermal fatigue on the residual strength of a laminate compared to mechanical fatigue.

- Specimen not loaded with any fatigue – Purpose: getting a strength baseline, while considering the deflection.
- Specimen only loaded with mechanical (tensile) fatigue – Purpose: getting a baseline of residual strength, while considering the deflection.
- Specimen loaded with thermal fatigue – Purpose: measure a difference in residual strength, while considering the deflection.
- Specimen loaded with thermal and mechanical (tensile) fatigue interchanging each other – Purpose: measure if there is interaction between thermal and mechanical fatigue, while considering the deflection.

The four test cases have to be done at different stages of the fatigue life cycle. This is because saturation of crack density can happen. Specimens from different tests can still have the same residual strength, if the difference in matrix cracks is not large. However, the stiffness (amount of deflection) can vary with small differences in crack density. Specimens with a high amount of cracks are more flexible and thus less stiff.

4.4.2 Manufacturing of coupons

First, a composite laminate has to be made, from which coupons can be machined. Pre-preg P707AG-15-1000 will be used to create a semi quasi-isotropic laminate $(45/-45/0/90/0/45/-45/90/0/90/45/-45/0)_s$. The material properties of a UD ply of P707AG-15-1000 can be found in appendix B.1. The stacking sequence is slightly dominant in the 0 degree direction. This is because normal composite structure are designed for a main load, but also have to withstand forces in off-axis directions. The pre-preg plies have a V_f of 54,4% and a theoretical cured ply thickness of 0,1524 mm of each ply. The whole laminate should be approximately 3,96 mm, however this can vary at different spots of the laminate due to manufacturing.

A cutting file (appendix B.2) was made to make sure the edges of each ply do not stack on top of each other. The edge dams and cover plate were cleaned with LPS Precision Cleaner and treated with Frekote 700-NC to ensure that the cleaning process after manufacturing is easier. The edge dams and cover plate are wrapped in A4000 release film. The plies are stacked from bottom to the top with plies of 600 mm by 500 mm with pre-compacting every 7 plies. The laminate will be cured in the autoclave. The autoclave package and program can be seen in appendix B.3 and B.4.

Before the coupons can be machined, a quality analysis of the laminate has to be performed. This has been done with a ultrasonic inspection (C-scan), which uses the damping of a signal through a laminate to measure the amount of defects or voids. The outcome can be seen in figure 4.3. Unfortunately, the laminate has a lot of defects or voids within it (the yellow and darker spots). The top left indication is not a void or defect, but a marker to determine the orientation of the laminate. Most of the defects are at the edges of internal plies. There could be multiple reasons why there are so many defects. It is possible that the pre-preg was too fast taken out of the bag, resulting in condensation at the edges of the pre-preg. Secondly, it is possible that the edges within one ply were not laid down accurately enough. A small gap between each edge could result in a void. Additionally, plies could be laid down with wrinkles, which can be seen in plies with the 0 direction, because those plies do not have any edges within one ply. Lastly, the autoclave program could not be sufficient enough for a good flow during the curing process. The most probable cause of the defects are the imperfections introduced while stacking the plies. The defects are precisely in a line within one ply and are following the fiber directions.

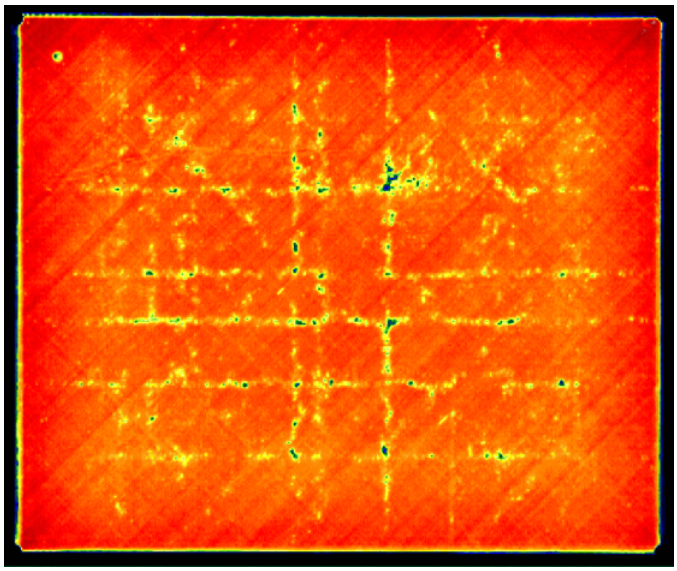

Figure 4.3: C-scan with defects of the laminate.

It is preferable to have test coupons without defects or voids. To solve this issue a precise machining scheme has to be made to reduce the amount of voids within a test coupon. Additionally, it could be used to identify test results that deviate from other results. The two major defect lines in the middle of the laminate in the 90 directions cannot be avoided. Coupons can not be cut closely from the edge due to a decreasing thickness at the edge. However, the major defects of the 90 directions are located at the edge of each coupon. This area will not be used during residual testing and is even part of the clamping area in the mechanical fatigue tests. Additionally, the defects in the 0 directions are mostly at the cutting line of the coupons. Unfortunately, it was not possible to avoid defects in each of the coupons. This should be considered, while analysing the results.

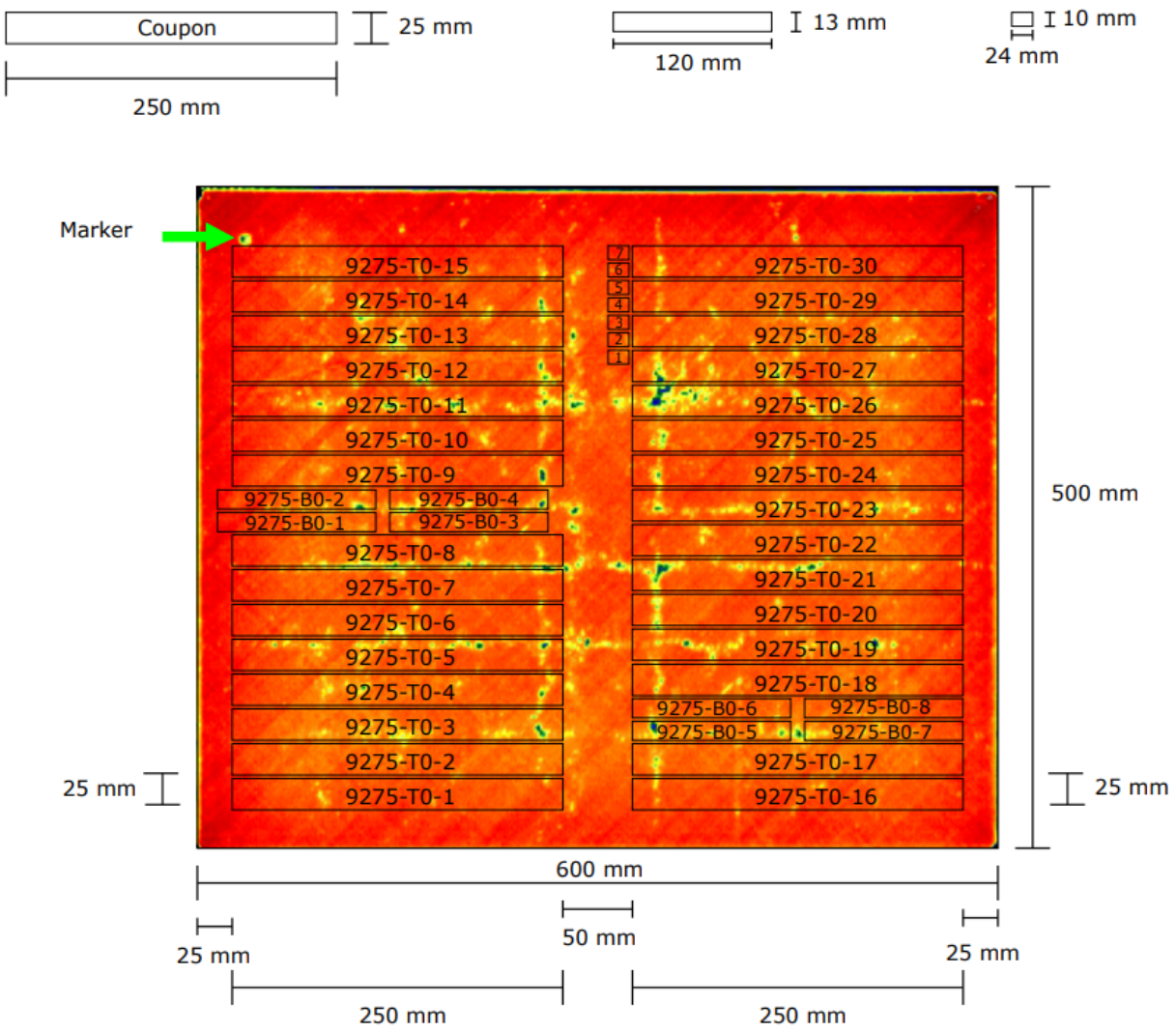

Figure 4.4: Machining scheme displayed onto the laminate with defects.

4.4.3 Mechanical fatigue test set up

To simulate mechanical in-service load a mechanical fatigue test will be performed. The test coupons consist of two reference sets and three fatigue testing sets. Two of the three testing coupons will be subjected to mechanical fatigue tests (table 4.3). One set of testing coupons will not endure mechanical fatigue, but only thermal fatigue. The last set (coupon number 21 up to 27) will be subjected to mechanical and thermal fatigue. Coupon number 28 to 30 will not be treated with mechanical or thermal fatigue. The reason for this will be explained in the next paragraph.

Table 4.3: Mechanical fatigue cycle plan.

Coupon	9275-T0-1	9275-T0-2	9275-T0-3	9275-T0-4	9275-T0-5
Coupon	9275-T0-21	9275-T0-22	9275-T0-23	9275-T0-24	9275-T0-25
Cycle counter	1.000	2.000	5.000	10.000	20.000
Coupon	9275-T0-6	9275-T0-7	9275-T0-8	9275-T0-9	9275-T0-10
Coupon	9275-T0-26	9275-T0-27			
Cycle counter	50.000	100.000	200.000	500.000	1.000.000

The mechanical fatigue test will be performed as much as a tension-tension fatigue test according to ASTM D3479 with a MTS 810 test bench. The specimen dimensions are approximately 3,9x25x250 mm. Using the maximum mechanical stress level of 117 MPa results in a maximum load of approximately 11.407 N, which will be rounded off to 11,5 KN. The ratio R will be use as 0.1, which gives a minimum load of 1,15 KN and a mean value of 6,325 KN. The test are performed at room temperature and this will be monitored during the fatigue test with a temperature sensor on the specimen. The clamping area on each side of the specimen is approximately 60 mm. Due to practicality (time restriction), a frequency of 2 or 3 Hz will be used. The test set-up is shown in figure 4.5.

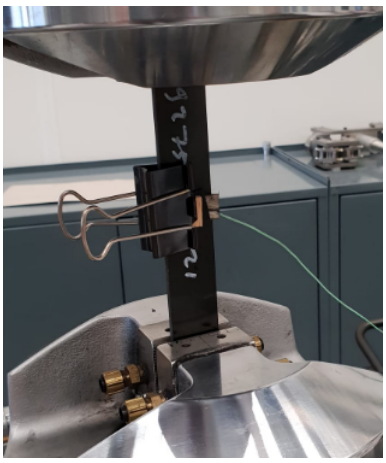

Figure 4.5: The mechanical fatigue test set up with temperature sensor on the coupon.

4.4.4 Thermal fatigue test set up

The thermal fatigue test will be performed after the mechanical fatigue test for planning purposes. The duration of the thermal fatigue test is long, especially the higher cycle counter. This is the reason that the last three coupons of each set will not be included into the test. The cycle counter of 1000, 2000, and ultimately 4000 (coupon number 18 to 20 and 28 to 30) would take to long to finish compared to the duration of the project, because a thermal cycle from 353K to 213K and back will take approximately 2 hours. The specimens are around 3,9 mm thick and needs time to fully adapt the temperature change in the centre of the specimen.

A climate chamber from Espec PSL-2KPH with a MSO-DAQ 1 temperature sensor will be used to apply the thermal fatigue load. Figure 4.6 displays a snapshot of the applied thermal load. When a cycle counter of a specific coupon has been reached, the coupon will be taken out of the chamber. Sometimes it was not possible to take the coupons out of the chamber at the exact cycle counter due to work hours, however the difference in cycle counter can be neglected.

Table 4.4: Thermal fatigue cycle plan.

Coupon	9275-T0-11	9275-T0-12	9275-T0-13	9275-T0-14	9275-T0-15	9275-T0-16	9275-T0-17
Coupon	9275-T0-21	9275-T0-22	9275-T0-23	9275-T0-24	9275-T0-25	9275-T0-26	9275-T0-27
Planned cycle counter	5	10	20	50	100	200	500
Actual cycle counter	5	11	20	50	102	199	504

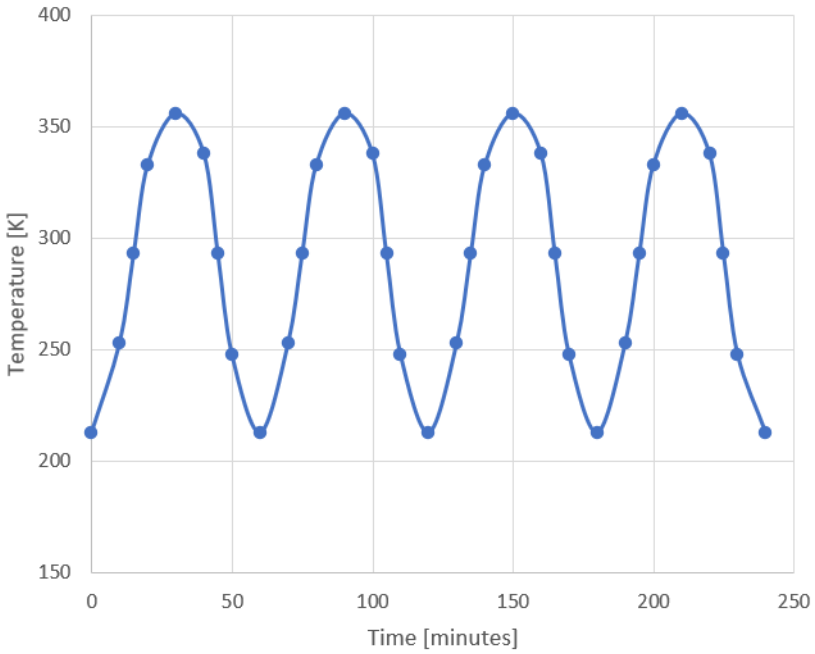

Figure 4.6: A snapshot of the thermal cycle applied on the coupons.

4.4.5 Residual bending strength set-up

To measure the influence of thermal and mechanical fatigue a bending test has been performed. In total 32 different bending coupons have to be tested. Eight of them are reference coupons, which were not subjected to fatigue loading and 24 were treated with mechanical and/or thermal fatigue (table 4.5 - 4.8). The test will be performed as much as possible according to ASTM D7264 four-points bending with an Instron 5900R test bench to measure the residual bending strength and stiffness. The dimension of the fatigue tested specimen is not according to the ASTM D7264.

Table 4.5: Reference set of the bending strength specimens.

Reference coupon	9275-B0-1	9275-B0-2	9275-B0-3	9275-B0-4	9275-B0-5	9275-B0-6	9275-B0-7	9275-B0-8
Mechanical cycle counter	0	0	0	0	0	0	0	0
Thermal cycle counter	0	0	0	0	0	0	0	0

Table 4.6: Set 1 of the bending strength specimens.

Coupon	9275-T0-1	9275-T0-2	9275-T0-3	9275-T0-4	9275-T0-5
Mechanical cycle counter	1.000	2.000	5.000	10.000	20.000
Thermal cycle counter	0	0	0	0	0
Coupon	9275-T0-6	9275-T0-7	9275-T0-8	9275-T0-9	9275-T0-10
Mechanical cycle counter	50.000	100.000	200.000	500.000	1.000.000
Thermal cycle counter	0	0	0	0	0

Table 4.7: Set 2 of the bending strength specimens.

Coupon	9275-T0-11	9275-T0-12	9275-T0-13	9275-T0-14	9275-T0-15	9275-T0-16	9275-T0-17
Mechanical cycle counter	0	0	0	0	0	0	0
Thermal cycle counter	5	10	20	50	102	199	504

Table 4.8: Set 3 of the bending strength specimens.

Coupon	9275-T0-21	9275-T0-22	9275-T0-23	9275-T0-24	9275-T0-25	9275-T0-26	9275-T0-27
Mechanical cycle counter	1.000	2.000	5.000	10.000	20.000	50.000	100.000
Thermal cycle counter	5	10	20	50	102	199	504

4-Points bending introduces a constant moment within the loading span, which is an advantage compared to 3 points bending, where the maximum bending moment occurs only at the loading point (figure 4.7). If the failure does not happen at the loading point in 3-points bending due to defects of centre, it is hard to determine the maximum failure load at a specific point of centre, while the area of maximum load in a 4-points bending test is much larger where the failure can occur. For this reason a 4-points bending test has been chosen. The support span during the test will be 80 mm with a loading span of 40 mm to correspond with the 25%-50% ratios mentioned in ASTM D7264. Four rollers with a diameter of 10 mm are used to ensure the rollers do not dent the specimen. In the middle of the specimen a displacement sensor is placed to measure the displacement during a test. The cross-head speed will be 2 mm per minute to have a test duration of approximately 3 minutes. The complete test set-up can be seen in appendix C.1.

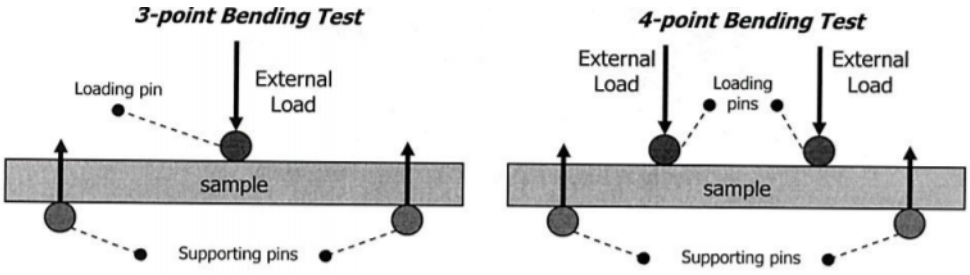

Figure 4.7: Diagram of 3 point and 4 point bending tests [22].

It is important to notice there is a dimension difference between the reference coupons and the mechanical/thermal fatigued coupons (figure B.5 and B.6) . The ASTM standard dimensions for bending are different compared to the dimensions of the tension-tension fatigue specimens, which results in a size difference. Tension-tension specimens are longer and wider than bending specimens. It is possible to resize the coupons that endured fatigue load, however this can cause negative side effects. As it is most likely that the coupons already have damage internally, it would be possible to introduce more damages and defects by resizing. Another consequence could be that the heat of the machining could meld the matrix and fill or "deburr" the cracks. Each side effect would influence the residual bending strength and stiffness. However, one cut will be necessary, because interlaminar shear specimens have to be made from the mechanical fatigue area (figure B.6). This cut does not influence the bending test, because it will be outside of the support span. The width of the specimen will influence the maximum load at failure. The flexural stress (formula 4.1) considers the width, therefore it is possible to compare the flexural stresses of the reference and fatigue specimens without considering other size-effects. Formula 4.2 is used to calculate the stiffness. The thickness and width will be determined for each coupon with an average at three different points of the coupon.

$$\sigma_{flexural} = \frac{3}{4} * \frac{P * L}{b * t^2} \tag{4.1}$$

Where
P = Maximum load at failure [N]
L = Support span [m]
b = Width of the specimen [m]
t = Thickness of the specimen [m]

$$K = \frac{P}{\delta} \tag{4.2}$$

Where
K = Stiffness [N/m]
P = Maximum load at failure [N]
δ = displacement [m]

4.4.6 Interlaminar shear strength set up

The second strength test will be an interlaminar shear strength test. Interlaminar shear strength is a matrix dominated failure mode. Thus, an increase of matrix cracks should result in a fast decrease of interlaminar shear strength. The test will be performed as much as possible according to ASTM D2344 (3-points bending, figure 4.7) with an Instron 5900R test bench. There are seven reference specimens and 48 fatigue coupons (table 4.9 - 4.12). The ILS coupons that are pre-tested with a fatigue load, have been machined from the large specimens (appendix B.5, figure B.5). This was necessary, because of the dimensions of the roller. The bottom rollers have a diameter of 3 mm and the top rollers has a diameter of 6 mm. Unfortunately, the rollers are 20 mm long, which means that the load would not be

applied uniformly if the specimen width is 25 mm during the test. This could result in failure modes, which are not explainable because the stress levels at the edges cannot be predicted. To avoid this the large fatigue coupons are machined into smaller ILS coupons of 3,9x11,5x24 mm. Each coupon will have three machined sides. Two of them are out side of the support span, but one edge (in the 0 direction) will be in the testing area. The cut could influence the results as described in the previous paragraph, however this is cut cannot be avoided.

Table 4.9: Reference set of the interlaminar shear strength specimens.

Reference coupon	1	2	3	4	5	6	7
Mechanical cycle counter	0	0	0	0	0	0	0
Thermal cycle counter	0	0	0	0	0	0	0

Table 4.10: Set 1 of the interlaminar shear strength specimens.

Coupon	ILS1.1	ILS2.1	ILS3.1	ILS4.1	ILS5.1	ILS6.1	ILS7.1	ILS8.1	ILS9.1	ILS10.1
Coupon	ILS1.2	ILS2.2	ILS3.2	ILS4.2	ILS5.2	ILS6.2	ILS7.2	ILS8.2	ILS9.2	ILS10.2
Mechanical cycle counter	1.000	2.000	5.000	10.000	20.000	50.000	100.000	200.000	500.000	1.000.000
Thermal cycle counter	0	0	0	0	0	0	0	0	0	0

Table 4.11: Set 2 of the interlaminar shear strength specimens.

Coupon	ILS11.1	ILS12.1	ILS13.1	ILS14.1	ILS15.1	ILS16.1	ILS17.1
Coupon	ILS11.2	ILS12.2	ILS13.2	ILS14.2	ILS15.2	ILS16.2	ILS17.2
Mechanical cycle counter	0	0	0	0	0	0	0
Thermal cycle counter	5	10	20	50	102	199	504

Table 4.12: Set 3 of the interlaminar shear strength specimens.

Coupon	ILS21.1	ILS22.1	ILS23.1	ILS24.1	ILS25.1	ILS26.1	ILS27.1
Coupon	ILS21.2	ILS22.2	ILS23.2	ILS24.2	ILS25.2	ILS26.2	ILS27.2
Mechanical cycle counter	1.000	2.000	5.000	10.000	20.000	50.000	100.000
Thermal cycle counter	5	10	20	50	102	199	504

The used test set-up can be seen in appendix C.2 figure C.3.The interlaminar shear strength will be calculated with formula 4.3. The thickness and width will be determined in the same matter as for the bending test. After failure, each specimen will be examined with a microscope to determine the failure mode as it will most likely not be visible for the naked eye.

$$\tau = \frac{3}{4} * \frac{P}{b * t} \tag{4.3}$$

Where
τ = Interlaminar shear strength [MPa]
P = Maximum load at failure [N]
b = Width of the specimen [m]
t = Thickness of the specimen [m]

Chapter 5

Experimental results

5.1 Bending results

5.1.1 Flexural strength

Figures 5.1 and 5.2 show the results of the flexural strength calculated with formula 4.1 based on the dimension measured of each coupon (appendix D). There is no clear decrease in strength at later stage of the fatigue life. The scatter of the reference set compared to set 1, 2, and 3 is looking the same (table 5.1). However, the average strength level from the reference set is different from the fatigue tested sets. The residual strength tests have been performed in the same manner, but the reference specimens did differ in size compared to the fatigue tested specimens. The difference in results are most likely caused by the difference in size of the specimens (the reference set specimens are shorter and narrower than the fatigue tested specimens), which is remarkable as equation 4.1 considers the size of a specimen. Three possible side-effects that could explain the difference in results are going to be discussed: edge effects, stress development, and a critical defect in a specimen.

The edge effects are probably not the cause of the difference in strength level. Figure 2.19 displays peak stresses at the edges. These peak stresses could lead to a decrease in strength value. However, the figure also explains that the edge effects are negligible after 1,5 times the thickness, which is around 6 mm in this case. Relative to the specimen width the edge effect has a larger influence on small specimens than on large specimens. A smaller specimen size would decrease the strength [23], however the results show an increase in strength. Another reason could be that the stress values cannot develop through the thickness of the coupons, but very short width (0,5 times the thickness) would be needed, which is also not the case. M.R. Winsom described the influence of the thickness of coupons on the bending strength [24]. The Weibull strength theory assumes that a critical defect will result in failure of the material. If there is more material, the chances are higher it has a critical defect. The same principle can be applied for different width sizes. A specimen with a large width has more chance to have a critical defect and thus will lead to a lower flexural strength [25], which is the behaviour of the bending results. Additionally, M.R. Winson reported that an increase

of specimen size in all directions leads to a reduction of material properties [26] identical to the results given in figure 5.1 and 5.2. Therefore, the latter effect is most likely the reason for the different results.

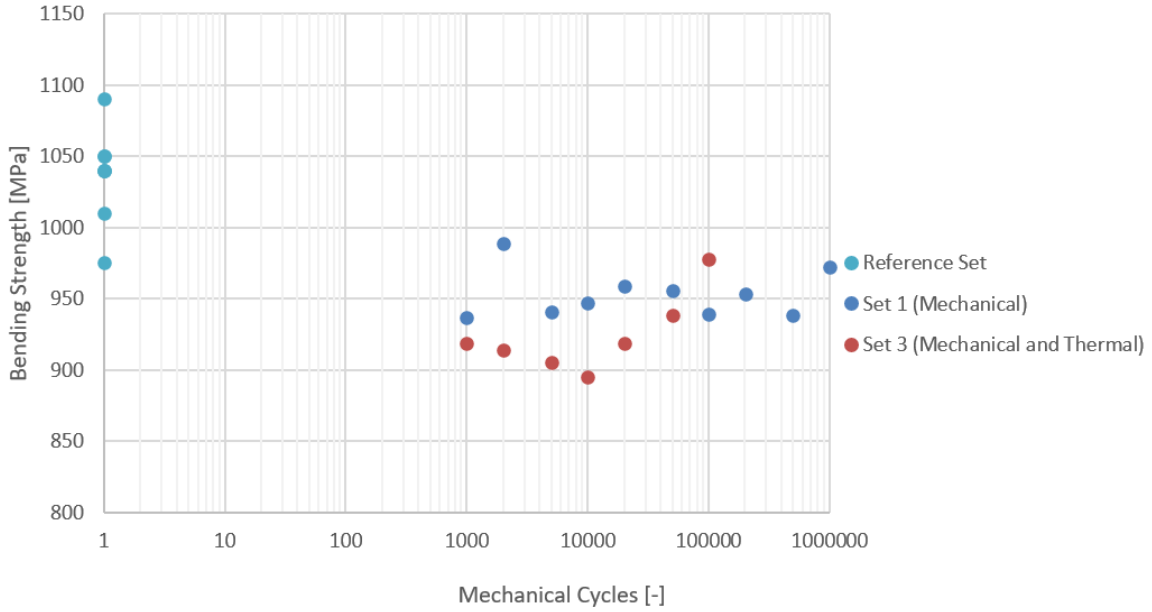

Figure 5.1: Residual bending strength of 3 different sets based on mechanical cycles.

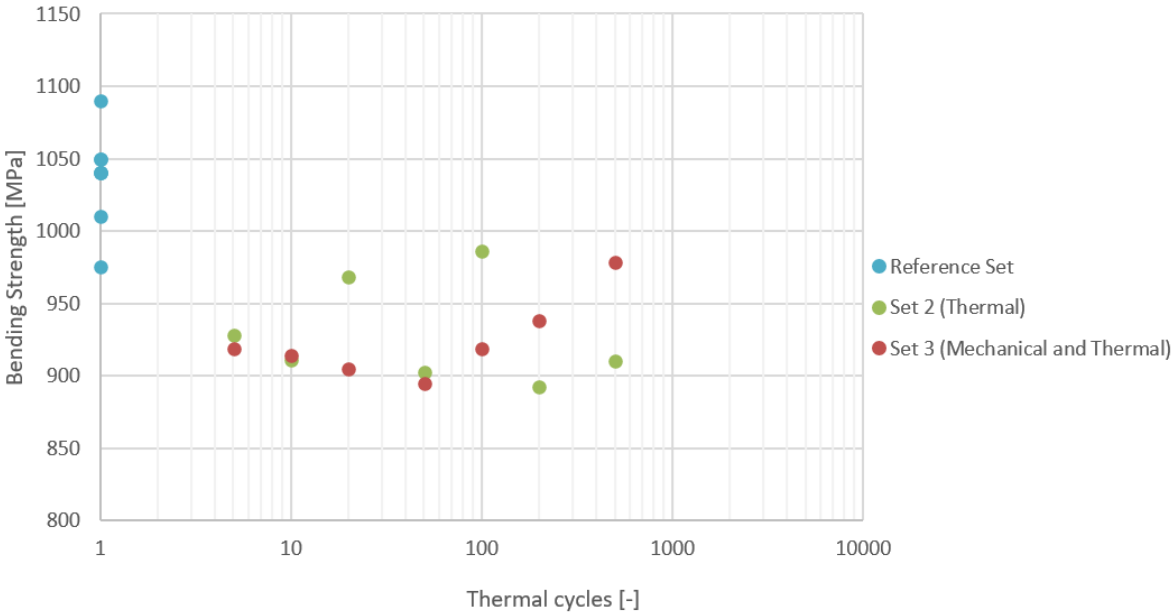

Figure 5.2: Residual bending strength of 3 different sets based on thermal cycles.

Table 5.1: The mean value, standard deviation an coefficient of variation of the bending results

	Flexural strength of reference coupons	Flexural strength of fatigue tested coupons
Mean value	1037 [MPa]	937 [MPa]
Standard deviation	33 [MPa]	29 [MPa]
Coefficient of variation	3.21 [%]	3.06 [%]

5.1.2 Failure modes

Based on the determined failure mode of each specimen (table D.9) a graph is made to see the difference in each set (figure 5.3). Immediately, a difference between the reference set and the fatigue tested sets is noticeable. The reference sets have more pure tension failure, while the other three sets have more multiple (tension and compression) failure modes. There is no clear change in the failure mode depending on the stage of fatigue life (table D.9). Using classical laminate theory and the average maximum load of the reference set (3,42KN) and of sets 1 till 3 (6,01KN) respectively gives for σ_{11} 2064 MPa and 1887 MPa (appendix D.3, figure D.2 and D.3), which is significantly higher than the compression strength S_{11c} as reported in figure B.1 of appendix B.1. The geometry of the specimen during bending (curved) creates additional support for the laminate, which results in a higher compression strength. The σ_{11} of 2064 MPa and 1887 MPa are just below the reported mean σ_{11t} (2172 MPa). There is no clear dissimilarity in compressive damage sizes of the fatigue tested sets (figure D.4). Thus, the multiple failure mode specimens are most likely failed in tension initially and the release of kinetic energy causes compression failure at the end. However, there is no explanation for the difference in the amount of the multiple failure mode of the reference coupons compared to the fatigue tested set. Interesting to see is the location of the failures (Appendix D.3, table D.9). If the failure happened at or near a loading point, it was most the times at the right-side of the loading span (figure 5.4). This is to be expected, because the right-side of the specimen is the centre area of the mechanical fatigue specimen. This area is furthest away from the clamping area and all mechanical fatigue stresses are fully developed in that area.

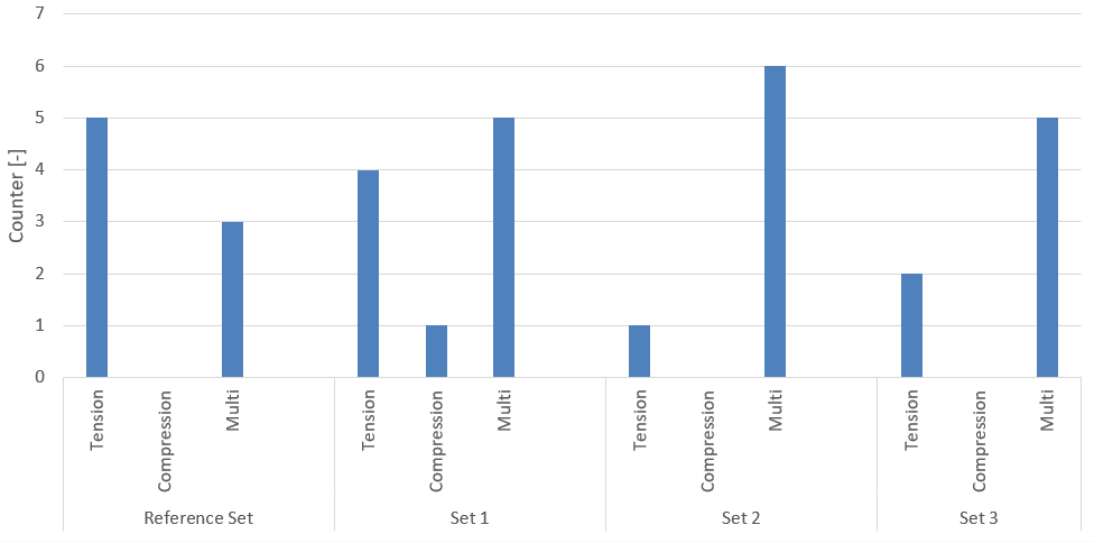

Figure 5.3: The amount of time a failure mode has occurred in a specific set.

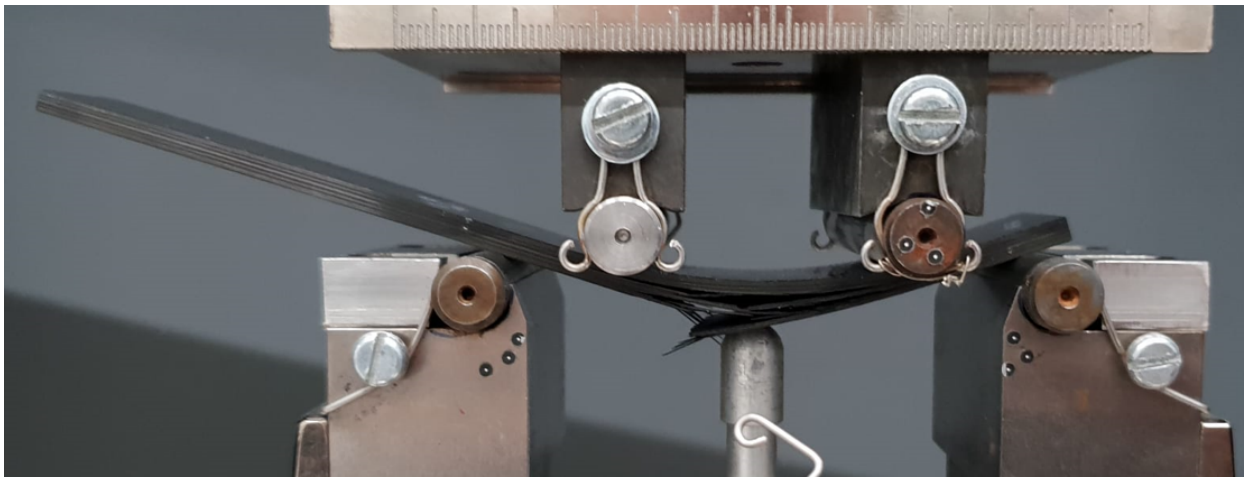

Figure 5.4: A failed specimen with a tension failure mode.

Figure 5.5: A close-up of a failed specimen with a tension failure mode.

5.1.3 Stiffness

Besides the maximum load, the displacement during the bending test was measured to determine the stiffness. Graphs in figure 5.6 and 5.7 are made with formula 4.2 divided by the width. Formula 4.2 can be used, if the dimensions of the coupons are the equal. However, if the dimensions of coupons are different, it is hard to compare the stiffness K, because the structural stiffness is also included in this value. To remove this factor, the stiffness K can be divided by the width to get a stiffness per width [N/mm/mm].

There is no clear sign of a decrease in stiffness per width based on figure 5.6 and 5.7. However, the graphs suggest two outliers (specimen 9275-T0-1 and 9275-T0-16). There is no explanation for these deviations, therefore the results of these two specimens should be considered. Table 5.2 shows that all values are close to each other, even with the two outliers included.

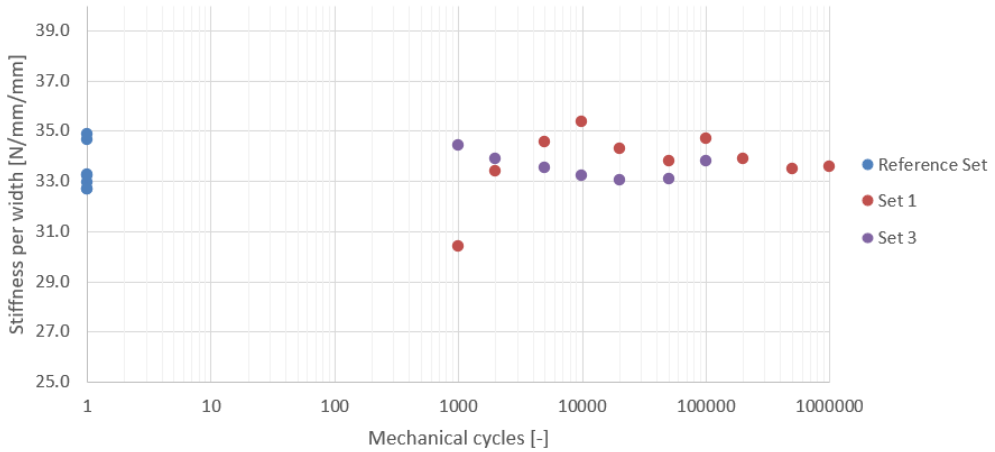

Figure 5.6: Stiffness per width of 3 different sets based on mechanical cycles

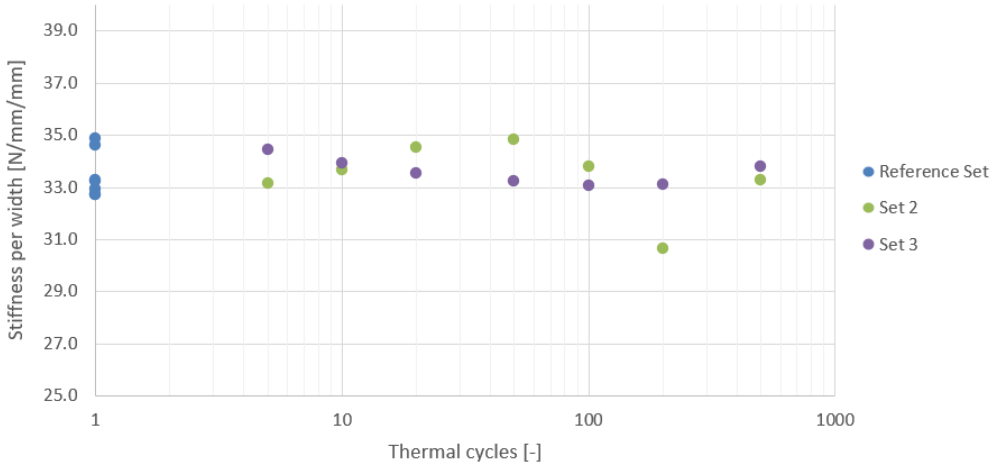

Figure 5.7: Stiffness per width of 3 different sets based on thermal cycles

Table 5.2: The mean value, standard deviation an coefficient of variation of the stiffness per width results.

	Stiffness of reference coupons	Stiffness of fatigue tested coupons
Mean value	33.43 [N/mm/mm]	33.61 [N/mm/mm]
Standard deviation	0.85 [N/mm/mm]	1.12 [N/mm/mm]
Coefficient of variation	2.53 [%]	3.34 [%]

5.2 Interlaminar Shear Results

5.2.1 Interlaminar Shear Strength

The interlaminar shear stresses are determined with formula 4.3 based on the measured coupon dimensions (appendix D). Figure 5.8 and 5.9 show the results displayed in a graph. The scatter of the fatigue tested coupons is larger compared to the reference coupon (table 5.3). Especially, the ones below a strength value of 75 MPa are standing out. There is no reason to assume these results are outliers. The location in the laminate where the specimens are cut from do not contain more voids or defects than other locations. However, the scatter of the AGATE results are close to the results of the fatigue tested coupons, which suggest that the void content of the fatigue tested coupons was approximately at qualification levels [27]. The mean value of the reference set, the fatigue tested sets and AGATE results are comparable with each other.

To determine whether the results of the reference and fatigue tested sets are different from each other, an equality of variance test with a two sided slope of 95% certainty is needed. However, the P value is only 0.11, which means there is no statistical argument to say the specimens results are different from each other. Thus, there is no reduction in residual interlaminar shear strength during different stages of the fatigue life.

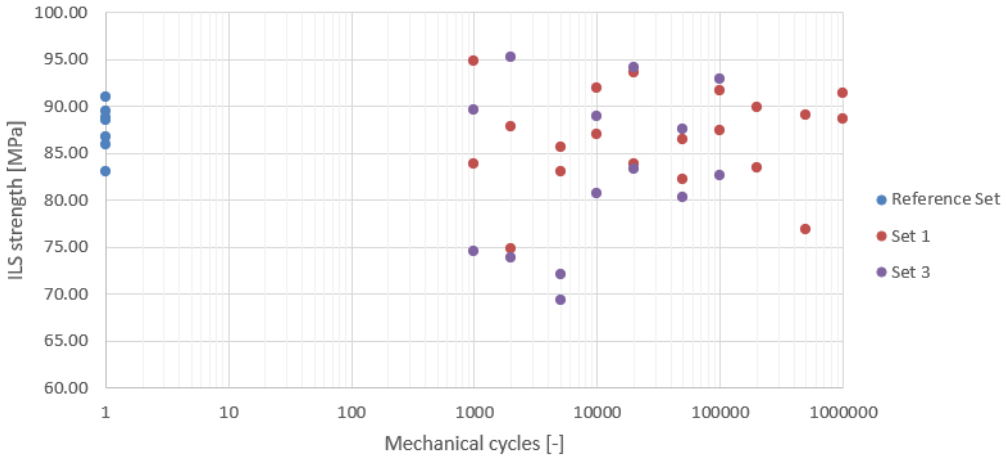

Figure 5.8: Residual interlaminar shear strength of 3 different sets based on mechanical cycles.

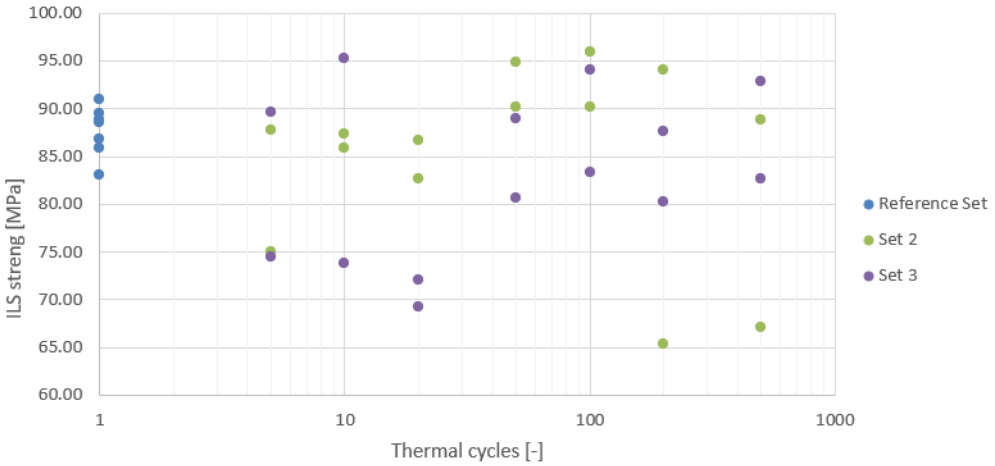

Figure 5.9: Residual interlaminar shear strength of 3 different sets based on thermal cycles.

Table 5.3: The mean value, standard deviation an coefficient of variation of the ILS results compared to the AGATE results [27].

	ILS of reference coupons	ILS of fatigue tested coupons	ILS results of AGATE
Mean value	87.66 [MPa]	85.2 [MPa]	86.108 [MPa]
Standard deviation	2.62 [MPa]	7.7 [MPa]	6.34 [MPa]
Coefficient of variation	2.99 [%]	8.98 [%]	7.368 [%]

5.2.2 Failure mode

The failure mode of each specimen is determined with a Leica MS5 microscope. All of the specimen failed in interlaminar shear (figure 5.10 and the cracks in each specimen are categorised (appendix D.4, figure D.5). Most of the cracks are located near the middle, but never within the 0 direction centre. Especially, the centre ±45 interface is dominant for ILS failure. Beside cracks between the 11^{th} and 12^{th} ply, cracks occurred between the 9^{th}, 10^{th}, and 11^{th} plies, which are a 0/90 and 90/45 interface. It is logical most of the failure occur near the middle of the specimen as the stresses built up towards the centre. It does not fail at the centre, because that is a strong 0/0 interface [28]. Interesting to notice is the peak of cracks at the interface of the sixth and seventh (±45 directions). This is a weak interface, however the stresses are low because of the location within the laminate. A possible explanation could be that after failure of the specimen in the centre, a "new" centre between the sixth and seventh ply is defined. Resulting in a build up of stresses at the weak interface, leading up to interlaminar shear cracks again.

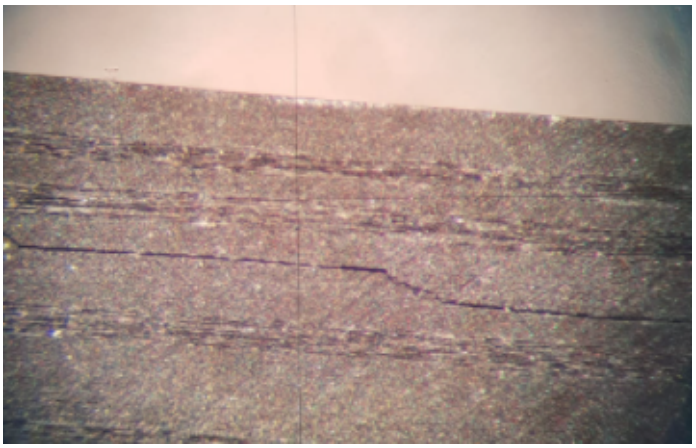

Figure 5.10: A close-up of a failed specimen with a interlaminar shear failure mode.

Chapter 6

Discussion

6.1 Research Questions

The results, given in the previous chapter, can be used to answer the three sub-questions and ultimately the main thesis question. Each question will be answered in each of the following paragraphs.

The results of the bending and interlaminar shear strength clearly show that a combination of mechanical and thermal fatigue does not have a negative impact on the material properties during the life cycle of a laminate. Additionally, the material properties do not degrade by the chosen thermal or mechanical fatigue load. This could mean that the chosen fatigue amplitude was not high enough to reduce the bending and the interlaminar shear strength of the laminate. This is conceivable, because real operational data of a F-16 has been used in the research, while the literature has shown difference but only in extreme conditions. This means that thermal and mechanical fatigue will not be issue during normal in-service operations.

Secondly, the stiffness of a laminate does not decrease after a mechanical and thermal fatigue load. As described for the residual strength, no significant change in bending stiffness per width was observed in the results. At the same time no reduction of stiffness has been found for specimens with only mechanical or only thermal fatigue. The same conclusion as for the residual bending and interlaminar shear strength can be made for the bending stiffness.

Thirdly, no decrease in residual bending and interlaminar shear strength has been observed at the different stages of the fatigue life. A remark should be made considering the end of life stage of thermal fatigue specimens. The last three specimen in the end of life stage of thermal fatigue are not tested due to the long duration of a thermal cycle. However, the results given in paragraph 5.1 show no indication of a decrease in material properties up to the last specimens. Therefore, it is to be expected that the material properties of the last three specimen are not affected by fatigue as well.

Lastly, the answers of the sub-questions ultimately lead up to the answer of the main question: "How will the structural integrity of a structure develop with a combined and realistic thermal

and mechanical load spectrum, applied during the life cycle of a representative laminate used in aerospace structures?". The results clearly show that the stiffness, residual bending and interlaminar shear strength do not decrease after a realistic combined thermal and mechanical applied load on a representative laminate used in aerospace structures. Therefore, it can be concluded there is no influence on the structural integrity, if the usage pattern and stresses are comparable to the applied loads.

6.2 Recommendations

During the thesis project choices were made that were acceptable, but not optimal for the results. To improve the experiment, the following improvements have to be made.

- A laminate with almost no defects or voids has to be manufactured as a base for the testing coupons. The machining scheme avoided these defects, but there were still some areas with voids within the specimens, which could have influenced the scatter of the results.
- One specimen size should be used for each strength test to avoid variations in results cause by dimension differences.
- Thermal fatigue coupons with higher cycle counter than 500 should be tested to validate the expectation that the structural integrity will not be influenced in the end stage of the life cycle.
- The amount of machining operations should be minimized to avoid damage introduction or the possibility of filling the cracks of damaged coupons.
- A greater a amount of test specimen is needed for a more profound statistical analysis.

Besides recommendation to validate and improve the results in this paper, further research considering thermal fatigue can be done. Especially, a research with other stacking sequences and thinner specimens, for example thin cross-ply laminates used in sandwich structures, in combination with a more severe fatigue load would be interesting for further operations.

Chapter 7

Conclusion

Thermal stresses in a composite are formed on three different levels: micro-mechanical, marco-mechanical, and laminate level. On each level thermal stresses are caused in different mechanisms, but they can all cause defects after a temperature change. Literature research has shown an increase of crack density in thermal fatigued cross-ply specimen at a lower cycle counter than mechanical fatigued cross-ply specimens in extreme environments. However, the crack density saturation level was the same for mechanical and thermal fatigue. However, the crack density is not the most important factor to consider during operational life. The structural integrity, the ability of a structure to perform it's function in a safe method, should be the dominant factor. Additionally, the extreme environmental conditions used in most published research programs are not common in normal aviation and the mechanical and thermal loads are applied simultaneously in-service and not separately.

The experiment performed, analysed the influence on transverse shear strength, residual bending strength, and stiffness of composite specimen that endured thermal and mechanical fatigue loads. The loads chosen were derived from F-16 data, to ensure the loads are in the order of magnitude as in normal aerospace operations. A semi-quasi isotropic laminate was made, because aircraft structures have to withstand multi-axial forces most of the time.

The results in paragraph 5.1 show no clear decrease of residual strength or stiffness at various stages of the life cycle caused by a fatigue load. The size differences of specimens have led to a difference in residual flexural strength. To conclude, the structural integrity will not be negatively influenced by a combination of thermal and mechanical fatigue, if the loads are similar during operations. Optimisation of the experimental test set-up is recommended as it could reduce the amount of scatter and confirm the assumptions made at the end stage of fatigue life. Additionally, further research on various stacking sequences, thinner specimens, and higher loads are advised to get an insight, if the reduction of structural integrity could happen in other manners.

Bibliography

[1] Dr. R. Alderliesten. *Fatigue of Structures and Materials*. University Lecture. 2019.

[2] Thomas Publishing Company. *A Brief History of Aircraft Materials*. (Accessed 11-12-2020). URL: https://www.thomasnet.com/insights/a-brief-history-of-aircraft-materials/.

[3] Anna G Koniuszewska and Jacek W Kaczmar. "Application of polymer based composite materials in transportation". In: *Progress in Rubber Plastics and Recycling Technology* 32.1 (2016), pp. 1–24.

[4] Dr. J. Sinke. *Fatigue of Structures and Materials*. University Lecture. 2019.

[5] Patricia P. Parlevliet, Harald E.N. Bersee, and Adriaan Beukers. "Residual stresses in thermoplastic composites—A study of the literature—Part I: Formation of residual stresses". In: *Composites Part A: Applied Science and Manufacturing* 37.11 (2006), pp. 1847–1857.

[6] Kevin D. Cowley and Peter W.R. Beaumont. "The measurement and prediction of residual stresses in carbon-fibre/polymer composites". In: *Composites Science and Technology* 57.11 (1997), pp. 1445–1455.

[7] Patricia P. Parlevliet, Harald E.N. Bersee, and Adriaan Beukers. "Residual stresses in thermoplastic composites – a study of the literature. Part III: Effects of thermal residual stresses". In: *Composites Part A: Applied Science and Manufacturing* 38.6 (2007), pp. 1581–1596.

[8] Q. Zhu et al. "Dimensional Accuracy of Thermoset Composites: Simulation of Process-Induced Residual Stresses." In: *Composite Materials* 35.24 (2001), pp. 2171–2205.

[9] Mathew W. Joosten et al. "Effect of residual stress on the matrix fatigue cracking of rapidly cured epoxy/anhydride composites". In: *Composites Part A: Applied Science and Manufacturing* 101 (2017), pp. 521–528.

[10] JA Barnes et al. "Thermal expansion behaviour of thermoplastic composite materials". In: *Journal of Thermoplastic Composite Materials* 3.1 (1990), pp. 66–80.

[11] Eric Leroy et al. "Evolution of the coefficient of thermal expansion of a thermosetting polymer during cure reaction". In: *Polymer* 46.23 (2005), pp. 9919–9927.

[12] G Baschek and G Hartwig. "Parameters influencing the thermal expansion of polymers and fibre composites". In: *cryogenics* 38.1 (1998), pp. 99–103.

[13] A. A. Fahmy and A. N. Ragai. "Thermal expansion of graphite-epoxy composites". In: *Journal of Applied Physics* 41 (1970).

[14] David A Spera. "What is thermal fatigue?" In: *Thermal fatigue of materials and components*. ASTM International, 1976.

[15] NL Hancox. "Thermal effects on polymer matrix composites: Part 1. Thermal cycling". In: *Materials & Design* 19.3 (1998), pp. 85–91.

[16] A Paillous and C Pailler. "Degradation of multiply polymer-matrix composites induced by space environment". In: *Composites* 25.4 (1994), pp. 287–295.

[17] C Arendt et al. "Long term durability testing of polymer composite materials". In: *12th International Conference on Composite Materials (ICCM12), Paris (France)*. 1999, pp. 5–9.

[18] Jaehyung Ju and Roger J Morgan. "Characterization of microcrack development in BMI-carbon fiber composite under stress and thermal cycling". In: *Journal of Composite Materials* 38.22 (2004), pp. 2007–2024.

[19] C Henaff-Gardin and MC Lafarie-Frenot. "Specificity of matrix cracking development in CFRP laminates under mechanical or thermal loadings". In: *International journal of fatigue* 24.2-4 (2002), pp. 171–177.

[20] MC Lafarie-Frenot and NQ Ho. "Influence of free edge intralaminar stresses on damage process in CFRP laminates under thermal cycling conditions". In: *Composites Science and Technology* 66.10 (2006), pp. 1354–1365.

[21] Satoshi Kobayashi et al. "Damage-mechanics analysis of matrix cracking in cross-ply CFRP laminates under thermal fatigue". In: *Composites science and technology* 61.12 (2001), pp. 1735–1742.

[22] S Sim and E Quenneville. "3-point or 4-point Bending Test". In: (2016).

[23] Hang Li et al. "Effects of specimen width on the tensile strength of aligned short-carbon-fiber reinforced epoxy composite laminates". In: *20th International Conference on Composite Materials, ICCM 2015*. 2015.

[24] Michael R. Wisnom. "The effect of specimen size on the bending strength of unidirectional carbon fibre-epoxy". In: *Composite Structures* 18.1 (1991), pp. 47–63.

[25] AR Chambers et al. "The effect of voids on the flexural fatigue performance of unidirectional carbon fibre composites developed for wind turbine applications". In: *International journal of fatigue* 28.10 (2006), pp. 1389–1398.

[26] M.R. Wisnom. "Size effects in the testing of fibre-composite materials". In: *Composites Science and Technology* 59.13 (1999), pp. 1937–1957.

[27] J Tomblin et al. "A – Basis and B – Basis Design Allowables for Epoxy – Based Prepreg TORAY T700GC-12K-31 Unidirectional Tape". In: (2002).

[28] R.J.C. Creemers. "Interlaminar shear strength criteria for composites". In: (2009).

Appendix A

Rule of Mixture

A.1 CTE of ply in fiber direction

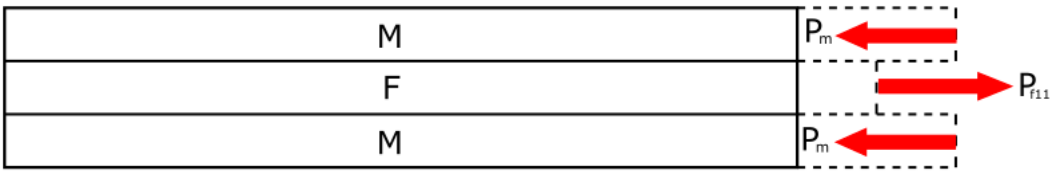

Figure A.1: A diagram of the thermal expansion causing tensile and compression forces within the ply, due to the boundary constrains of the fiber and matrix layers.

The formula below can be derived from figure A.1.

$$\Delta L_m = \Delta T * \alpha_m * L_0 - \frac{P_m}{A_m * E_m} * L_0 \tag{A.1}$$

And

$$\Delta L_f = \Delta T * \alpha_{f11} * L_0 + \frac{P_f}{A_f * E_m} * L_0 \tag{A.2}$$

Translate to strain will give

$$\epsilon_m = \Delta T * \alpha_m - \frac{P_m}{A_m * E_m} \tag{A.3}$$

And

$$\epsilon_f = \Delta T * \alpha_{f11} + \frac{P_f}{A_f * E_f} \tag{A.4}$$

ϵ_m, ϵ_f, and ϵ_{11} should be equal due to boundary constrains.

$$\epsilon_f = \epsilon_m = \epsilon_{11} \tag{A.5}$$

The sum of the forces is zero due to an equilibrium state.

$$P_f = P_m \tag{A.6}$$

Using formula A.5 to combine formula A.4 and A.3 gives

$$\Delta T * \alpha_m - \frac{P_m}{A_m * E_m} = \Delta T * \alpha_{f11} + \frac{P_f}{A_f * E_f} \tag{A.7}$$

Which can be derived further

$$\Delta T * \alpha_m - \Delta T * \alpha_{f11} = \frac{P_f}{A_f * E_f} + \frac{P_m}{A_m * E_m} \tag{A.8}$$

Using A.6 gives

$$\Delta T(\alpha_m - \alpha_{f11}) = P_m \frac{1}{A_f * E_f} + \frac{1}{A_m * E_m} \tag{A.9}$$

$$\Delta T(\alpha_m - \alpha_{f11}) = P_m \frac{A_f * E_f + A_m * E_m}{A_f * E_f * A_m * E_m} \tag{A.10}$$

$$\frac{A_f * E_f * A_m * E_m}{A_f * E_f + A_m * E_m} * \Delta T(\alpha_m - \alpha_{f11}) = P_m \tag{A.11}$$

$$\frac{A_f * E_f}{\frac{A_f}{A_m} * \frac{E_f}{E_m} + 1} * \Delta T(\alpha_m - \alpha_{f11}) = P_m \tag{A.12}$$

The surface of the fiber and matrix can be translate to a volume fraction with the thickness of the ply.

$$V_f = \frac{A_f}{t} \tag{A.13}$$

And

$$V_m = \frac{A_m}{t} \tag{A.14}$$

Therefore

$$\frac{A_f}{A_m} = \frac{V_f}{V_m} \tag{A.15}$$

Substituting this in formula A.12 gives

$$\frac{A_f * E_f}{\frac{V_f}{V_m} * \frac{E_f}{E_m} + 1} * \Delta T(\alpha_m - \alpha_{f11}) = P_m \tag{A.16}$$

This can be substituted in formula A.4 using A.6

$$\epsilon_f = \Delta T * \alpha_{f11} + \frac{1}{A_f * E_f} * \frac{A_f * E_f}{\frac{V_f}{V_m} * \frac{E_f}{E_m} + 1} * \Delta T(\alpha_m - \alpha_{f11}) \tag{A.17}$$

$$\epsilon_f = \Delta T * \alpha_{f11} + \frac{1}{\frac{V_f}{V_m} * \frac{E_f}{E_m} + 1} * \Delta T(\alpha_m - \alpha_{f11}) \tag{A.18}$$

The strain for a ply can be written as

$$\epsilon_{11} = \Delta T * \alpha_{11} \tag{A.19}$$

This can be substitute in A.18 using A.5

$$\Delta T * \alpha_{11} = \Delta T * \alpha_{f11} + \frac{1}{\frac{V_f}{V_m} * \frac{E_f}{E_m} + 1} * \Delta T(\alpha_m - \alpha_{f11}) \tag{A.20}$$

$$\alpha_{11} = \alpha_{f11} * (1 - \frac{1}{\frac{V_f}{V_m} * \frac{E_f}{E_m} + 1}) + \alpha_m * \frac{1}{\frac{V_f}{V_m} * \frac{E_f}{E_m} + 1} \tag{A.21}$$

The volume fraction of the fiber and matrix added up should be 1.

$$V_f + V_m = 1 \tag{A.22}$$

This can be substituted in the equation A.21 giving the CTE of a unidirectional ply in the fiber direction.

$$\alpha_{11} = \alpha_{f11} * (1 - \frac{1}{\frac{V_f}{1-V_f} * \frac{E_f}{E_m} + 1}) + \alpha_m * \frac{1}{\frac{V_f}{1-V_f} * \frac{E_f}{E_m} + 1} \tag{A.23}$$

$$\alpha_{11} = \alpha_{f11} * \frac{\frac{V_f}{1-V_f} * \frac{E_f}{E_m}}{\frac{V_f}{1-V_f} * \frac{E_f}{E_m} + 1} + \alpha_m * \frac{1}{\frac{V_f}{1-V_f} * \frac{E_f}{E_m} + 1} \tag{A.24}$$

$$\alpha_{11} = \alpha_{f11} * \frac{1}{\frac{1-V_f}{V_f} * \frac{E_m}{E_f} + 1} + \alpha_m * \frac{1}{\frac{V_f}{1-V_f} * \frac{E_f}{E_m} + 1} \tag{A.25}$$

Additionally, it is possible to derive the formula of the force further to stresses.

$$\frac{A_f * E_f}{\frac{A_f}{A_m} * \frac{E_f}{E_m} + 1} * \Delta T(\alpha_m - \alpha_{f11}) = P_m \tag{A.26}$$

The force in the matrix is a compression force and in the fiber tension.

$$\sigma_m = \frac{-P_m}{A_m} \tag{A.27}$$

$$\sigma_f = \frac{-P_f}{A_f} \tag{A.28}$$

Giving

$$\frac{\frac{-A_f}{A_m} * E_f}{\frac{A_f}{A_m} * \frac{E_f}{E_m} + 1} * \Delta T(\alpha_m - \alpha_{f11}) = \sigma_m \tag{A.29}$$

$$\frac{E_f}{\frac{A_f}{A_m} * \frac{E_f}{E_m} + 1} * \Delta T(\alpha_m - \alpha_{f11}) = \sigma_f \tag{A.30}$$

Using formula A.15 gives

$$\frac{\frac{-V_f}{1-V_f} * E_f}{\frac{V_f}{1-V_f} * \frac{E_f}{E_m} + 1} * \Delta T(\alpha_m - \alpha_{f11}) = \sigma_m \tag{A.31}$$

$$\frac{-E_m}{1 + \frac{1-V_f}{V_f} * \frac{E_m}{E_f}} * \Delta T(\alpha_m - \alpha_{f11}) = \sigma_m \tag{A.32}$$

And

$$\frac{E_f}{\frac{V_f}{1-V_f} * \frac{E_f}{E_m} + 1} * \Delta T(\alpha_m - \alpha_{f11}) = \sigma_f \tag{A.33}$$

A.2 CTE of ply in transverse direction

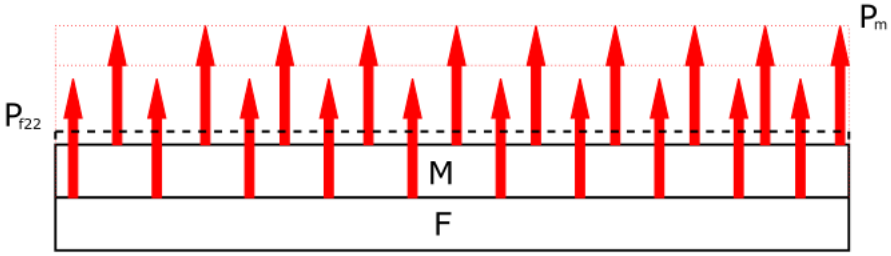

Figure A.2: A diagram of the thermal expansion and the internal forces within a ply, due to a thermal change.

The formula below can be derived from figure A.2.

$$\Delta L_m = \Delta T * \alpha_m * t_m \tag{A.34}$$

And

$$\Delta L_f = \Delta T * \alpha_{f22} * t_f \tag{A.35}$$

the volume faction for the matrix and fiber can be written as

$$V_m = \frac{t_m}{t_m + t_f} \tag{A.36}$$

And

$$V_f = \frac{t_f}{t_m + t_f} \tag{A.37}$$

Where

$$t_0 = t_m + t_f \tag{A.38}$$

This can be substituted in the expansion equations A.34 and A.35.

$$\Delta L_m = \Delta T * \alpha_m * V_m * t_0 \tag{A.39}$$

And

$$\Delta L_f = \Delta T * \alpha_{f22} * V_f * t_0 \tag{A.40}$$

The expansion of each layer can be added up to get the expansion of the ply

$$\Delta L_{22} = \Delta L_m + \Delta L_f \tag{A.41}$$

giving

$$\Delta L_{22} = \Delta T * \alpha_m * V_m * t_0 + \Delta T * \alpha_{f22} * V_f * t_0 \tag{A.42}$$

Which can be translate to strain of a ply

$$\epsilon_{22} = \Delta T * \alpha_m * V_m + \Delta T * \alpha_{f22} * V_f \tag{A.43}$$

The thermal expansion can also be written as

$$\epsilon_{22} = \Delta T * \alpha_{22} \tag{A.44}$$

This can be substituted into equation A.43 to get

$$\Delta T * \alpha_{22} = \Delta T * \alpha_m * V_m + \Delta T * \alpha_{f22} * V_f \tag{A.45}$$

$$\alpha_{22} = \alpha_m * V_m + \alpha_{f22} * V_f \tag{A.46}$$

Appendix B

Manufacturing of the laminate

B.1 Material properties of P707AG-15-1000

UD ply properties*				
		AGATE		NLR
		Mean value	B-basis value	Measurement
S_{11T}	[MPa]	2172	1912	--
E_{11T}	[GPa]	125.5	--	126.0
S_{11C}	[MPa]	1450	1281	--
E_{11C}	[GPa]	112.3	--	109.3
S_{22T}	[MPa]	48.9	42.8	--
E_{22T}	[GPa]	8.406	--	8.683
S_{22C}	[MPa]	198.7	180.3	242.5
E_{22C}	[GPa]	10.139	--	9.254
S_{12}	[MPa]	154.7	145.5	97.0
G_{12}	[GPa]	4.229	--	4.839
S_{13}	[MPa]	86.1	76.8	91.8
G_{13}	[GPa]	--	--	4.993
S_{23}	[MPa]	--	--	--
G_{23}	[GPa]	--	--	2.724
ν_{12}	[-]	0.309	--	--

* Properties are normalized to a nominal cured ply thickness of 0.1524 mm (corresponding to V_f=54.4%).

Figure B.1: The material properties of a UD P707AG-15-1000 ply.

B.2 Cutting layout of prepreg

Figure B.2: The cutting layout of the prepreg.

B.3 Autoclave package

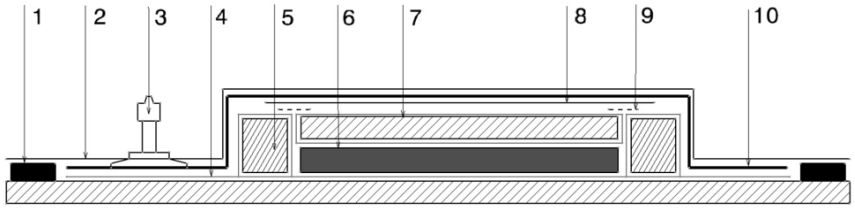

1	Tacky tape, GS213-3	6	Panels
2	Vacuum foil IPPLON DP1000	7	Cover plate wrapped up in A4000
3	Vacuümpoint (2x)	8	Glass fabric SS0303 stopping halfway the edge dams
4	A4000 release film	9	A4000 pin pricked every 30 mm on the edge between edge dam and cover plate. Use tape to fix the A4000 in order to keep the holes aligned with the cover plate and edge dams.
5	Edge dam wrapped in A4000	10	Breather Airweave Super 10 (2x)

Figure B.3: A diagram of the autoclave package.

B.4 Autoclave program

Programma		Start stop	Operation	Operation	Operation	Operation	Operation	Operation	Operation	Start stop
	Segment time	00:00:00	00:01:30	00:32:30	00:01:30	00:01:36	00:02:18	00:16:12	02:00:00	00:27:51
	Temp. [°C]	20	23.8	88.8	91.8	95	99.6	132	132	54
	Press. [bar]	0	0.3	0.3	1.05	1.85	3	3	3	3
	Vac. [bar]	0	-0.95	-0.95	-0.95	-0.15	-0.15	-0.15	-0.15	-0.15
	Temp.Check	☐	☐	☐	☐	☐	☐	☐	☑	☐

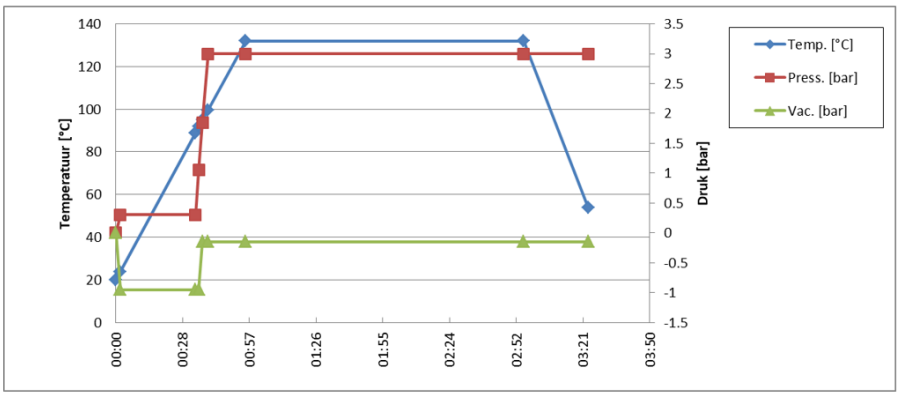

Figure B.4: A diagram of the autoclave curing program.

B.5 Static and fatigue test coupons

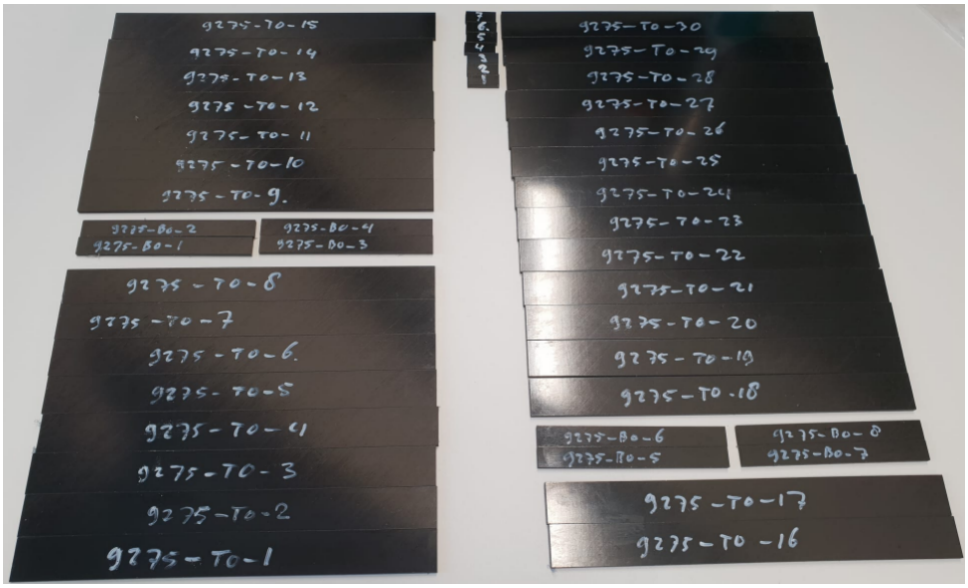

Figure B.5: Test coupons cut from a laminate for fatigue testing.

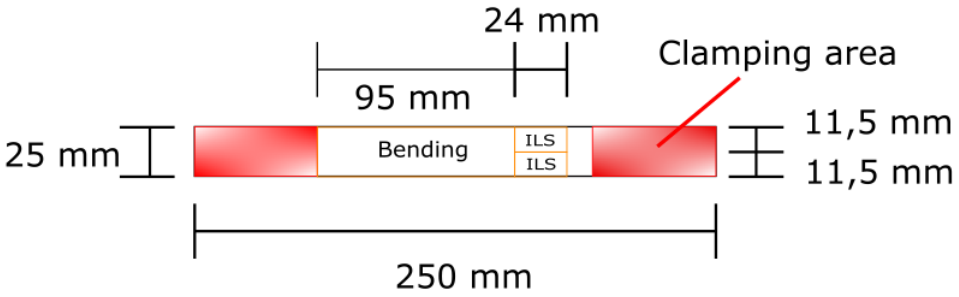

Figure B.6: A schematic diagram of the bending and ILS specimens.

Appendix C

Bending and ILS test set-up

C.1 Bending test set-up

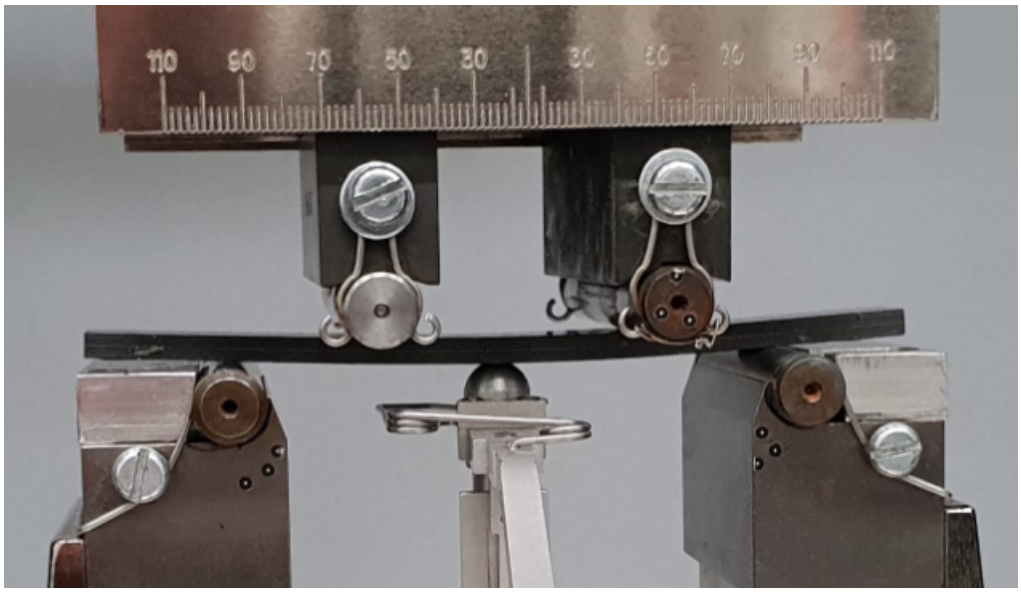

Figure C.1: The bending test set-up for the reference coupons.

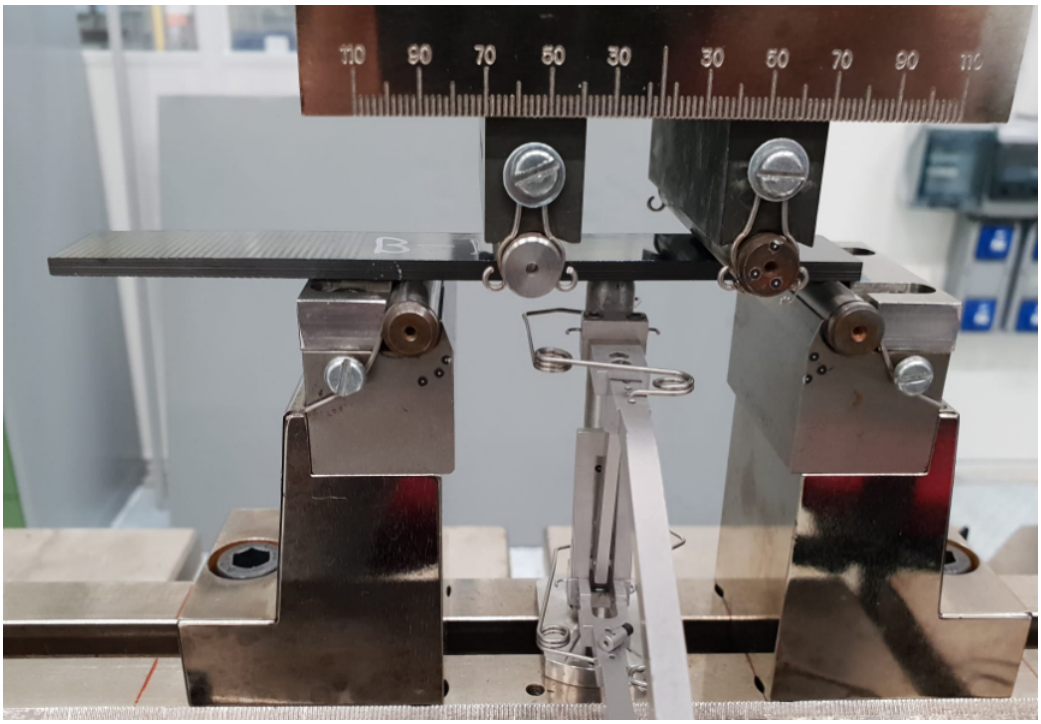

Figure C.2: The bending test set-up for the fatigue tested coupons.

C.2 ILS test set-up

Figure C.3: The ILS test set-up.

Appendix D

Results Data

D.1 Dimensional data of bending specimens

Table D.1: Dimensional data of reference bending coupons.

Coupon	Thickness 1 [mm]	Thickness 2 [mm]	Thickness 3 [mm]	Average thickness [mm]
9275-B0-1	3.577	3.946	3.927	3.817
9275-B0-2	3.601	3.945	3.922	3.823
9275-B0-3	3.912	3.915	3.913	3.913
9275-B0-4	3.905	3.923	3.921	3.916
9275-B0-5	3.952	3.951	3.937	3.947
9275-B0-6	3.963	3.961	3.940	3.955
9275-B0-7	3.954	3.990	3.751	3.898
9275-B0-8	3.965	3.993	3.763	3.907
Coupon	Width 1 [mm]	Width 2 [mm]	Width 3 [mm]	Average width [mm]
9275-B0-1	13.04	13.02	13.03	13.03
9275-B0-2	13.05	13.03	13.03	13.03
9275-B0-3	13.03	13.03	13.03	13.03
9275-B0-4	13.03	13.03	13.02	13.03
9275-B0-5	13.02	13.03	13.03	13.03
9275-B0-6	13.03	13.02	13.03	13.02
9275-B0-7	13.03	13.04	13.05	13.04
9275-B0-8	13.03	13.03	13.01	13.02

Table D.2: Dimensional data of set 1 of the bending coupons.

Coupon	Thickness 1 [mm]	Thickness 2 [mm]	Thickness 3 [mm]	Average thickness [mm]
9275-T0-1	3.818	3.789	3.713	3.773
9275-T0-2	3.863	3.860	3.912	3.878
9275-T0-3	4.003	3.988	3.938	3.976
9275-T0-4	4.008	3.976	3.933	3.972
9275-T0-5	3.987	3.951	3.918	3.952
9275-T0-6	3.971	3.932	3.901	3.935
9275-T0-7	3.963	3.945	3.904	3.937
9275-T0-8	3.971	3.940	3.907	3.939
9275-T0-9	3.971	3.936	3.904	3.937
9275-T0-10	3.963	3.922	3.897	3.927
Coupon	Width 1 [mm]	Width 2 [mm]	Width 3 [mm]	Average width [mm]
9275-T0-1	25.10	25.09	25.09	25.09
9275-T0-2	25.04	25.05	25.05	25.05
9275-T0-3	25.03	25.04	25.03	25.03
9275-T0-4	25.03	25.02	25.02	25.02
9275-T0-5	25.01	25.02	25.02	25.02
9275-T0-6	25.04	25.03	25.03	25.03
9275-T0-7	25.03	25.02	25.02	25.03
9275-T0-8	25.14	25.15	25.14	25.14
9275-T0-9	24.90	24.91	24.91	24.90
9275-T0-10	25.00	25.00	25.00	25.00

Table D.3: Dimensional data of set 2 of the bending coupons.

Coupon	Thickness 1 [mm]	Thickness 2 [mm]	Thickness 3 [mm]	Average thickness [mm]
9275-T0-11	3.942	3.910	3.881	3.911
9275-T0-12	3.943	3.929	3.888	3.920
9275-T0-13	3.979	3.949	3.928	3.952
9275-T0-14	3.984	3.955	3.926	3.955
9275-T0-15	3.948	3.913	3.864	3.908
9275-T0-16	3.750	3.756	3.764	3.757
9275-T0-17	3.910	3.889	3.913	3.904
Coupon	Width 1 [mm]	Width 2 [mm]	Width 3 [mm]	Average width [mm]
9275-T0-11	25.04	25.04	25.03	25.04
9275-T0-12	25.02	25.02	25.02	25.02
9275-T0-13	25.02	25.02	25.02	25.02
9275-T0-14	25.02	25.02	25.02	25.02
9275-T0-15	25.04	25.03	25.03	25.03
9275-T0-16	24.79	24.80	24.81	24.80
9275-T0-17	25.26	25.25	25.24	25.25

Table D.4: Dimensional data of set 3 of the bending coupons.

Coupon	Thickness 1 [mm]	Thickness 2 [mm]	Thickness 3 [mm]	Average thickness [mm]
9275-T0-21	3.924	3.923	3.946	3.931
9275-T0-22	3.970	3.950	3.929	3.950
9275-T0-23	3.914	3.919	3.952	3.928
9275-T0-24	3.906	3.914	3.944	3.921
9275-T0-25	3.922	3.904	3.938	3.921
9275-T0-26	3.950	3.904	3.935	3.930
9275-T0-27	3.974	3.937	3.927	3.946
Coupon	Width 1 [mm]	Width 2 [mm]	Width 3 [mm]	Average width [mm]
9275-T0-21	25.02	25.02	25.01	25.02
9275-T0-22	25.02	25.02	25.02	25.02
9275-T0-23	25.02	25.02	25.02	25.02
9275-T0-24	25.11	25.10	25.09	25.10
9275-T0-25	24.73	24.72	24.72	24.72
9275-T0-26	25.25	25.24	25.24	25.25
9275-T0-27	25.02	25.02	25.02	25.02

D.2 Dimensional data of ILS specimens

Table D.5: Dimensional data of reference ILS coupons.

Coupon	Thickness 1 [mm]	Thickness 2 [mm]	Thickness 3 [mm]	Average thickness [mm]
1	3.932	3.926	3.923	3.927
2	3.957	3.953	3.950	3.953
3	3.905	3.905	3.901	3.904
4	3.874	3.873	3.874	3.874
5	3.833	3.826	3.824	3.828
6	3.758	3.757	3.754	3.757
7	3.676	3.648	3.656	3.660
Coupon	Width 1 [mm]	Width 2 [mm]	Width 3 [mm]	Average width [mm]
1	10.02	10.02	10.02	10.02
2	10.01	10.01	10.00	10.01
3	10.02	10.03	10.02	10.02
4	10.03	10.03	10.03	10.03
5	10.02	10.01	10.01	10.01
6	10.02	10.01	10.01	10.01
7	10.05	10.05	10.05	10.05

Table D.6: Dimensional data of set 1 of the ILS coupons.

Coupon	Thickness 1 [mm]	Thickness 2 [mm]	Thickness 3 [mm]	Average thickness [mm]
ILS1.1	3.761	3.763	3.766	3.763
ILS1.2	3.666	3.663	3.662	3.664
ILS2.1	3.894	3.901	3.900	3.898
ILS2.2	3.958	3.954	3.949	3.954
ILS3.1	3.936	3.935	3.938	3.936
ILS3.2	3.933	3.926	3.929	3.929
ILS4.1	3.928	3.927	3.924	3.926
ILS4.2	3.933	3.932	3.933	3.933
ILS5.1	3.902	3.906	3.903	3.904
ILS5.2	3.911	3.915	3.917	3.914
ILS6.1	3.911	3.908	3.906	3.908
ILS6.2	3.906	3.908	3.907	3.907
ILS7.1	3.905	3.901	3.902	3.903
ILS7.2	3.905	3.902	3.902	3.903
ILS8.1	3.899	3.900	3.896	3.898
ILS8.2	3.900	3.900	3.896	3.899
ILS9.1	3.892	3.889	3.890	3.890
ILS9.2	3.894	3.888	3.892	3.891
ILS10.1	3.884	3.882	3.882	3.883
ILS10.2	3.89	3.887	3.893	3.890
Coupon	Width 1 [mm]	Width 2 [mm]	Width 3 [mm]	Average width [mm]
ILS1.1	11.80	11.80	11.80	11.80
ILS1.2	11.52	11.52	11.52	11.52
ILS2.1	11.77	11.78	11.78	11.77
ILS2.2	11.51	11.52	11.51	11.52
ILS3.1	11.81	11.81	11.84	11.81
ILS3.2	11.47	11.47	11.46	11.47
ILS4.1	11.81	11.81	11.81	11.81
ILS4.2	11.46	11.45	11.45	11.45
ILS5.1	11.79	11.78	11.78	11.78
ILS5.2	11.47	11.47	11.46	11.47
ILS6.1	11.81	11.81	11.80	11.81
ILS6.2	11.48	11.47	11.48	11.48
ILS7.1	11.81	11.81	11.81	11.81
ILS7.2	11.45	11.45	11.45	11.45
ILS8.1	11.80	11.80	11.80	11.80
ILS8.2	11.60	11.60	11.59	11.60
ILS9.1	11.79	11.80	11.80	11.80
ILS9.2	11.34	11.35	11.33	11.34
ILS10.1	11.81	11.81	11.82	11.80
ILS10.2	11.44	11.44	11.434	11.44

Table D.7: Dimensional data of set 2 of the ILS coupons.

Coupon	Thickness 1 [mm]	Thickness 2 [mm]	Thickness 3 [mm]	Average thickness [mm]
ILS11.1	3.883	3.879	3.874	3.879
ILS11.2	3.881	3.879	3.878	3.879
ILS12.1	3.920	3.913	3.919	3.917
ILS12.2	3.898	3.891	3.887	3.892
ILS13.1	3.921	3.915	3.918	3.918
ILS13.2	3.921	3.917	3.919	3.919
ILS14.1	3.925	3.918	3.918	3.920
ILS14.2	3.924	3.926	3.922	3.924
ILS15.1	3.850	3.851	3.853	3.851
ILS15.2	3.893	3.893	3.897	3.894
ILS16.1	3.823	3.826	3.826	3.825
ILS16.2	3.739	3.732	3.736	3.736
ILS17.1	3.944	3.944	3.943	3.944
ILS17.2	3.902	3.902	3.903	3.902
Coupon	Width 1 [mm]	Width 2 [mm]	Width 3 [mm]	Average width [mm]
ILS11.1	11.81	11.81	11.80	11.81
ILS11.2	11.47	11.47	11.46	11.46
ILS12.1	11.80	11.80	11.80	11.80
ILS12.2	11.45	11.45	11.45	11.45
ILS13.1	11.82	11.81	11.80	11.82
ILS13.2	11.46	11.46	11.46	11.46
ILS14.1	11.79	11.79	11.79	11.79
ILS14.2	11.47	11.47	11.47	11.47
ILS15.1	11.81	11.81	11.81	11.81
ILS15.2	11.46	11.46	11.46	11.46
ILS16.1	11.81	11.81	11.80	11.80
ILS16.2	11.26	11.25	11.25	11.25
ILS17.1	11.80	11.80	11.80	11.80
ILS17.2	11.70	11.70	11.70	11.70

Table D.8: Dimensional data of set 3 of the ILS coupons.

Coupon	Thickness 1 [mm]	Thickness 2 [mm]	Thickness 3 [mm]	Average thickness [mm]
ILS21.1	3.956	3.955	3.953	3.955
ILS21.2	3.952	3.947	3.950	3.950
ILS22.1	3.913	3.910	3.911	3.911
ILS22.2	3.908	3.908	3.910	3.909
ILS23.1	3.957	3.956	3.950	3.954
ILS23.2	3.955	3.956	3.954	3.955
ILS24.1	3.947	3.943	3.949	3.946
ILS24.2	3.946	3.949	3.948	3.948
ILS25.1	3.938	3.934	3.934	3.935
ILS25.2	3.935	3.932	3.936	3.934
ILS26.1	3.943	3.936	3.938	3.939
ILS26.2	3.933	3.939	3.931	3.934
ILS27.1	3.982	3.949	3.944	3.958
ILS27.2	3.936	3.929	3.931	3.932
Coupon	Width 1 [mm]	Width 2 [mm]	Width 3 [mm]	Average width [mm]
ILS21.1	11.81	11.81	11.81	11.81
ILS21.2	11.46	11.46	11.46	11.46
ILS22.1	11.80	11.80	11.80	11.80
ILS22.2	11.45	11.45	11.45	11.45
ILS23.1	11.80	11.80	11.80	11.80
ILS23.2	11.48	11.48	11.48	11.48
ILS24.1	11.82	11.82	11.81	11.81
ILS24.2	11.55	11.56	11.55	11.55
ILS25.1	11.78	11.78	11.78	11.78
ILS25.2	11.17	11.18	11.18	11.18
ILS26.1	11.80	11.80	11.80	11.80
ILS26.2	11.69	11.68	11.68	11.68
ILS27.1	11.81	11.81	11.81	11.81
ILS27.2	11.46	11.47	11.46	11.46

D.3 Bending failure modes

Table D.9: Bending failure modes with characters based on figure D.1.

Coupon	9275-B0-1	9275-B0-2	9275-B0-3	9275-B0-4	9275-B0-5
Failure mode	MAV	MAV	TAB	TBB	MAV
Coupon	9275-B0-6	9275-B0-7	9275-B0-8		
Failure mode	TAB	TAB	TBB		
Coupon	9275-T0-1	9275-T0-2	9275-T0-3	9275-T0-4	9275-T0-5
Failure mode	TBB	TBB	MAV	TAB	TBB
Coupon	9275-T0-6	9275-T0-7	9275-T0-8	9275-T0-9	9275-T0-10
Failure mode	MAV	MAV	CAL	MAV	MAV
Coupon	9275-T0-11	9275-T0-12	9275-T0-13	9275-T0-14	9275-T0-15
Failure mode	MAV	MAV	MAV	MAV	TAR
Coupon	9275-T0-16	9275-T0-17			
Failure mode	MAV	MAV			
Coupon	9275-T0-21	9275-T0-22	9275-T0-23	9275-T0-24	9275-T0-25
Failure mode	MAV	MBV	MAV	MBV	TBB
Coupon	9275-T0-26	9275-T0-27			
Failure mode	TBB	MAV			

First Character

Failure Mode	Code
Tension	T
Compression	C
Buckling	B
interlaminar Shear	S
Multi-mode	M(xyz)
Other	O

Second Character

Failure Area	Code
At loading nose	A
Between loading noses	B
at Support nose	S
between Load and support nose	L
Unknown	U

Third Character

Failure Location	Code
Top	T
Bottom	B
Left	L
Right	R
Middle	M
Various	V
Unknown	U

Figure D.1: Failure modes characters used in table D.9.

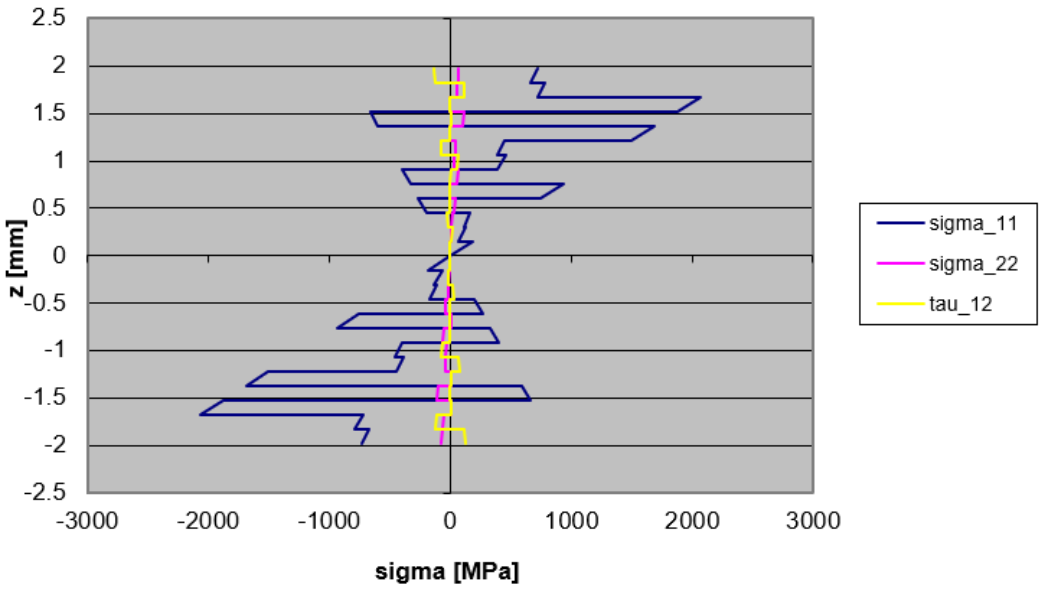

Figure D.2: Stress levels of each ply throughout the thickness of the reference coupons calculated with the classical laminate theory.

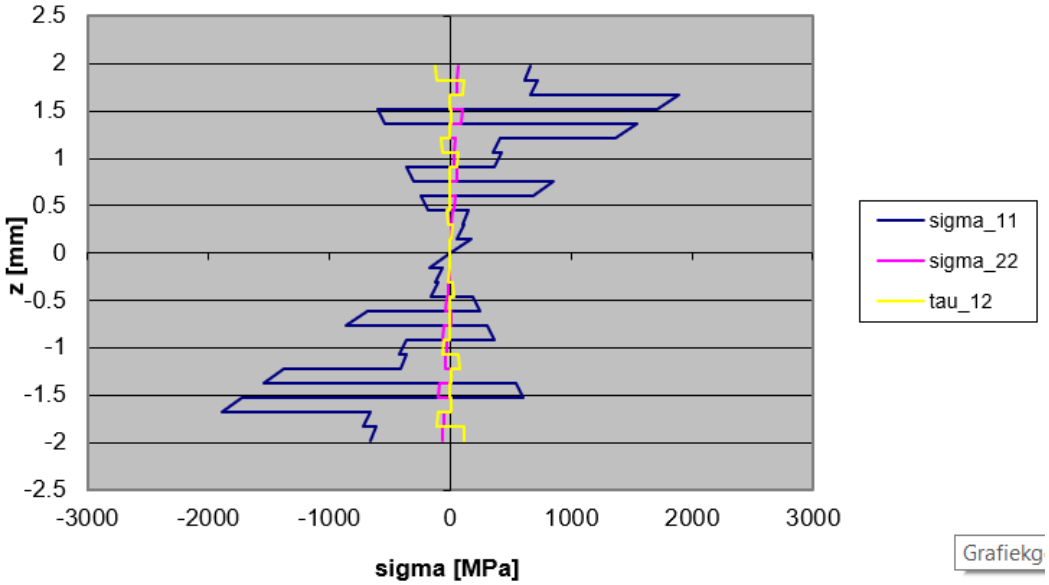

Figure D.3: Stress levels of each ply throughout the thickness of the fatigue tested coupons calculated with the classical laminate theory.

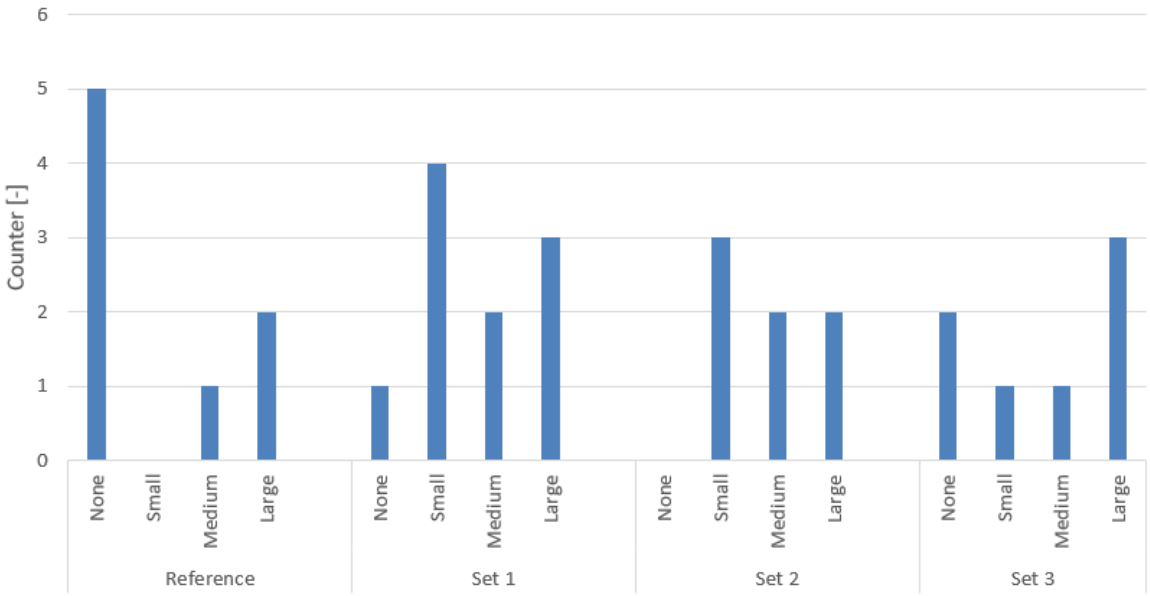

Figure D.4: Size of compression damage for each set.

D.4 ILS failure modes

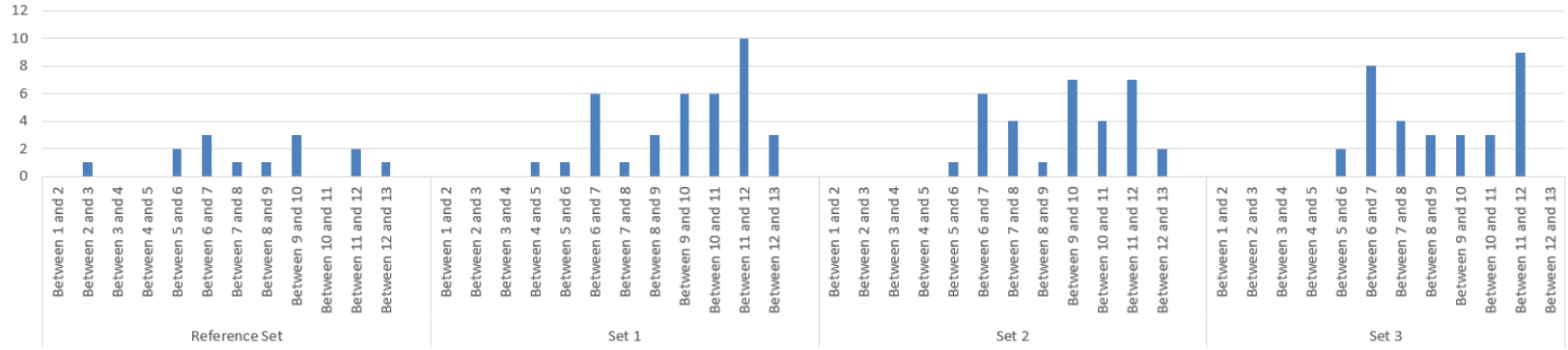

Figure D.5: The amount of ILS cracks between specific plies for each set.